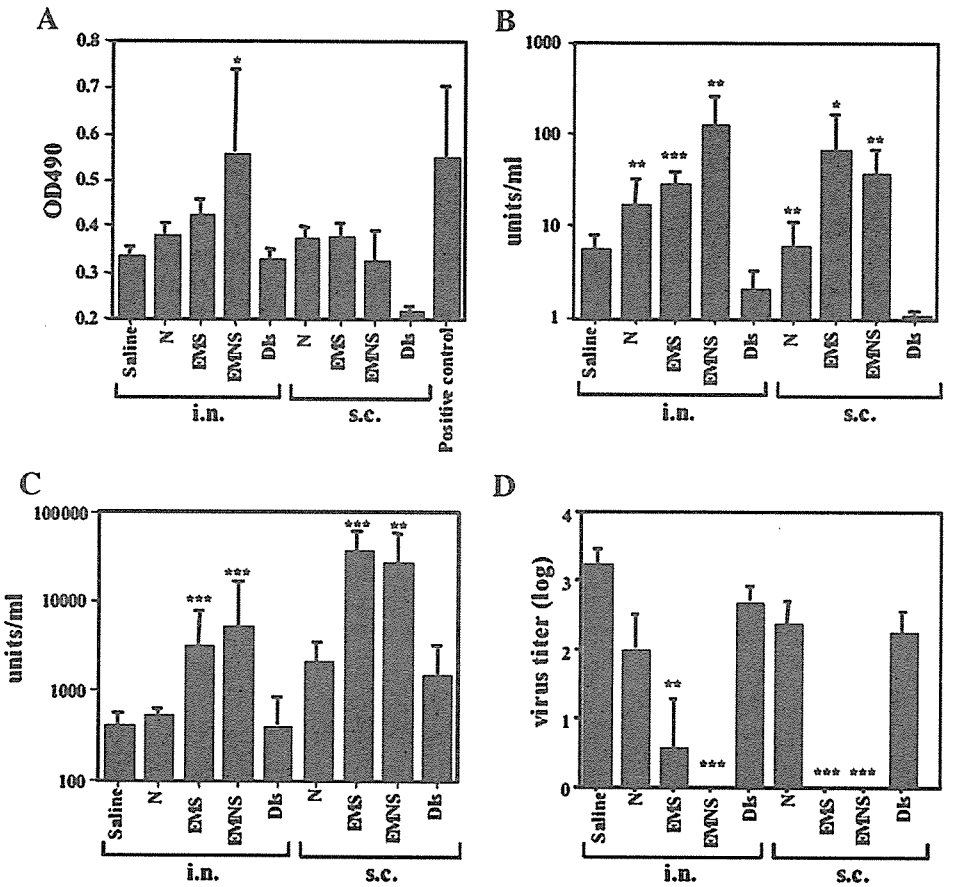

Fig. 4. Mucosally secreted anti-SARS-CoV IgG, but not IgA, antibodies are protective from nasal SARS-CoV challenge in vaccinated mice. The levels of Ig A and IgG antibodies against SARS-CoV were determined as described in Materials and methods. (A) Titers of anti-SARS-CoV IgA in the nasal washings of vaccinated mice. Error bars represent the mean ± SD. (B) Titers of anti-SARS-CoV IgG in the nasal washings of vaccinated mice. Error bars represent the mean ± SD. (C) Titers of anti-SARS-CoV IgG in the sera of vaccinated mice. Error bars represent the mean ± SD. (D) The titers of SARS-CoV in the lungs of vaccinated mice challenged 1 week later with 10^4 $TCID_{50}$ of SARS-CoV. Virus titers are expressed as $\log_{10}TCID_{50}$. Error bars represent the mean ± SD. $^*P < 0.1$, $^{**}P < 0.05$, $^{***}P < 0.01$ vs. DIs-administered group.

Notably, mice immunized with rDIsSARS-S produced a high level of IFN-γ upon in vitro stimulation with UV-inactivated, purified SARS-CoV virion. The production of TNF-α, an inflammatory cytokine, was significantly elevated in T cells in ALN of rDIsSARS-S immunized mice after in vitro stimulation with virion antigens. However, TNF-α production was observed also in mice immunized with parental DIs without in vitro stimulation with virion antigens. Since T cells from the

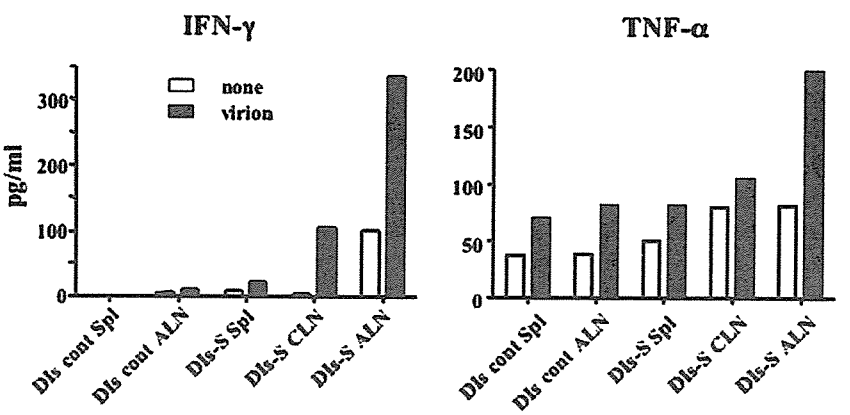

Fig. 5. In vitro response of SARS-CoV-specific T cells in mice subcutaneously immunized with rDIsSARS-S. CLN, ALN and spleens were obtained from mice 1 week after the third vaccination of either DIs control or rDIsSARS-S. After preparation of single cell suspensions, T cells were purified and cultivated with irradiated and T-cell depleted normal BALB/c mouse splenocytes as APCs in the presence or absence of 10 μg/ml of purified UV-irradiated SARS-CoV virion. Four days later, IFN-γ and TNF-α concentrations in the culture supernatant were measured.

lymph nodes of naïve mice did not produce cytokines even after in vitro stimulation with virion antigens (data not shown), it is possible that injection of DIs induces mild local inflammation, even when viral proliferation does not occur at the injection site. The pattern of IL-2, IL-5 and IL-4 production were similar to that of IFN-γ, and the maximum level of these cytokines in ALN T cells from rDIsSARS-S-immunized mice were 254, 227 and 88 ng/ml, respectively.

Next, we analyzed the antigenic epitopes of SARS-CoV-specific T cells in the spleen. We carried out IFN-γ enzyme-linked immunospot (ELISPOT) analysis using four 20-mer peptides corresponding to the ACE2 binding region of the S protein selected using the SYFPEITHI score (S44-47), as well as overlapping 20-mer peptides pool covering a whole N protein. When the splenic T cells of mice were analyzed following intranasal or subcutaneous immunization with the most potent vaccine, rDIsSARS-E/M/N/S, a high level of reactivity against S46 was observed especially in the T cells of subcutaneously immunized mice (Fig. 6A). Zhi et al. recently identified a $CD4^+$ T cell epitope, known as NYNYKYRYL, in BALB/c mice (Zhi et al., 2005). S46 contains this sequence, thus, these IFN-γ-producing T cells are likely $CD4^+$ T cells. To detect N-specific T cells, mice subcutaneously or intranasally immunized with rDIsSARS-N were analyzed by ELISPOT. In this case, ten peptides were pooled from amino-terminus of N protein, resulting in 5 pools of peptides. We thus detected N-reactive T cells capable of recognizing the first 10 peptides pool (Fig. 6B), and observed a greater proportion of N-specific T cells following nasal immunization than subcutaneous immunization. These results indicate that S- and N-specific T cells are generated systemically by rDIs.

In order to elucidate whether or not SARS-CoV-specific $CD8^+$ T cells were induced by immunization with the rDIs, the splenic T cells of mice subcutaneously or intranasally immunized with rDIsSARS-E/M/N/S were further analyzed by ELISPOT using a stably S-expressing A20.2J B cell S6.2 clone, as an antigen presenting cells (APC). Expression of S protein on the S6.2 clone was confirmed by FACS analysis using anti-SARS S monoclonal antibody (Fig. 7A). An empty vector transfectant, BOS-5, was used as a negative control APC. Subcutaneous and intranasal immunization with the most potent rDIsSARS-E/M/N/S generated a significant level of S-specific T cells (Fig. 7B), and a dramatic decrease in S-specific T cells was observed following partial depletion of $CD8^+$ T cells (Fig. 7C). Therefore, rDIsSARS-E/M/N/S was able to induce both SARS-CoV-reactive $CD4^+$ and $CD8^+$ T cells.

Histopathological findings

The immunogenicity of rDIs expressing SARS-CoV structural proteins was further evaluated by histopathological and immunohistochemical analysis of lung tissue in mice, the primary infection site of SARS-CoV (Fig. 8). Slight migration of inflammatory cells and mild disruption of the bronchial epithelium were detected in lung tissue of mock-vaccinated mice. SARS-CoV antigens were diffusely observed within the bronchial and alveolar epithelium. In contrast, significant lymphocytic infiltration into peribronchial sites, with little to no detection of SARS-CoV antigens, was observed in mice intranasally immunized with rDIsSARS-E/M/S or rDIsSARS-E/M/N/S (Fig. 8). The infiltrating lymphocytes were found to be CD3-positive T-cells, as determined by immunohistochemistry with anti-CD3 antibody (Fig. 8). On the other hand, intranasal or subcutaneous immunization by only N-expressing DIs induced neither T-cell infiltration nor protective immunity against SARS-CoV, despite of the induction of N-specific antibodies and T cells. These results suggest that marked induction of T-cell response in mice immunized with rDIsSARS-E/M/S and rDIsSARS-E/M/N/S help to eliminate SARS-CoV from the lung tissue. On the other hand, intranasal or subcutaneous immunization by only N-expressing DIs did not induce protective immunity against SARS-CoV, despite of the

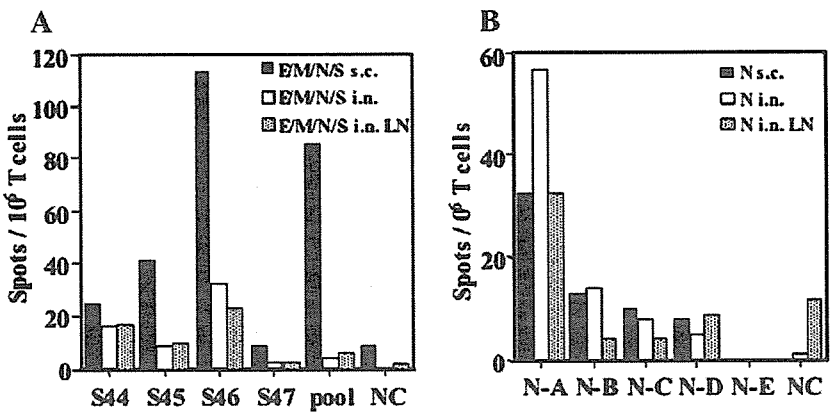

Fig. 6. Detection of SARS-CoV-specific T cells elicited by rDIsSARS-E/M/N/S or rDIsSARS-N vaccination. Splenic and lymph node (LN) T cells of mice s.c. or i.n. immunized with recombinant rDIsSARS-E/M/N/S (A) or rDIsSARS-N (B) were separated using a MACS system (Miltenyi Biotec), and IFN-γ ELISPOT analysis was performed. (A) T cells (5×10^5 cells) from mice immunized with rDIsSARS-E/M/N/S were cultured with irradiated A20.2J B cells (1×10^4), in triplicate, in a 96-well membrane plates coated with IFN-γ capture antibody in the absence or presence of 5 μM of S peptides (S44–S47). The numbers of IFN-γ spot-forming cells were then counted and are depicted. (B) T cells from mice immunized with rDIsSARS-N and A20.2J B cells were cultured as described in A. N protein (422 amino acids) was divided into 5 parts by 100 amino acids (A, B, C, D and E) and 10 peptides each of pooled 20-mer overlapping peptides specific to the each stretch of N sequence were used as an antigen.

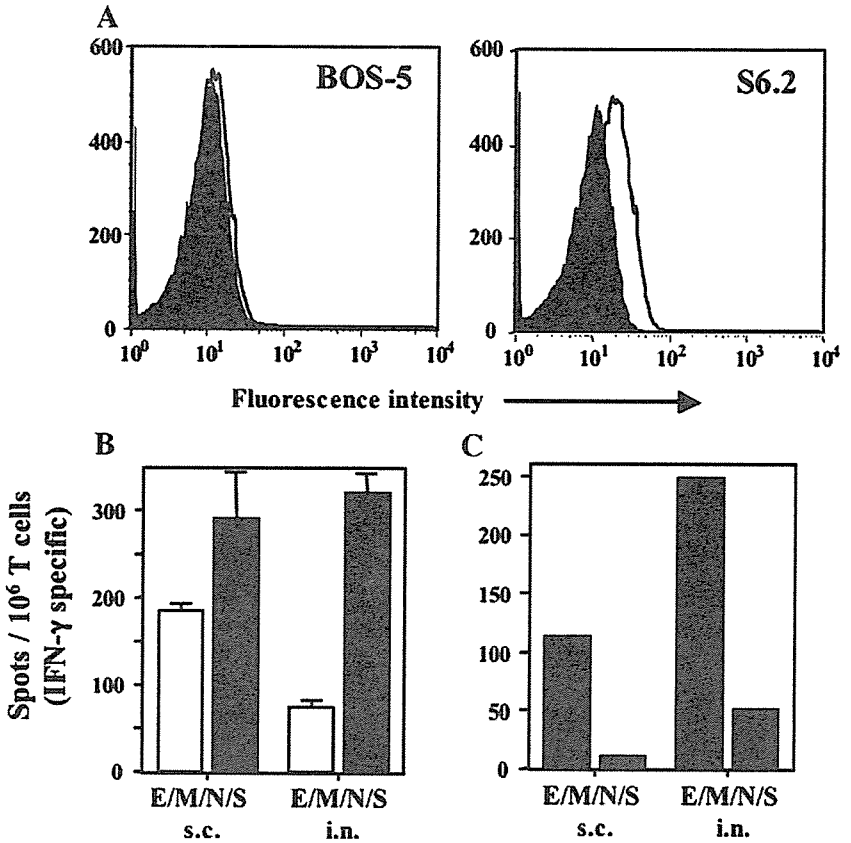

Fig. 7. Detection of SARS-CoV S-specific $CD8^+$ T cells in mice immunized with rDIsSARS-E/M/N/S. (A) A20.2J B cell clone expressing S (S6.2) or empty vector (BOS-5) was stained with biotinylated anti-SARS-CoV S monoclonal antibody (solid line) or control IgG (shadowed line), followed by the incubation with streptavidin-APC, and then analyzed by FACScalibur. A histogram of APC fluorescence of gated live cells (PI negative) is depicted. (B) Splenic T cells from mice immunized s.c. or i.n. with recombinant rDIsSARS-E/M/N/S were purified and IFN-γ ELISPOT analysis was carried out using γ-irradiated S6.2 and BOS-5 as APCs. The number of T cells reactive for BOS-5 control (white column) and S6.2 (black column) cells are shown. Error bars represent the mean ± SD. (C) Using the same splenic T cells as in panel B, $CD8^+$ T cells were partially removed using anti-CD8 mAb-coated magnetic beads (Miltenyi Biotec), and the number of T cells reactive for BOS-5 and S6.2 cells were counted by ELISPOT. The number of BOS-5-reactive T cells was subtracted and the number of S-specific T cells is depicted. Black columns: total T cells; grey columns: partially CD8-depleted T cells.

induction of N-specific antibodies and T cells. Thus, rDIs expressing the S protein, along with other membrane components (E/M and E/M/N), are capable of inducing strong immunity of both humoral and cellular arms and are fully competent to clear SARS-CoV infection.

Discussion

The DIs strain, which replicates well in CEF cells but not in most mammalian cells, was isolated from the DIE strain of the vaccinia virus during serial 1-day egg passage, and it is characterized by the induction of tiny pocks on chicken chorioallantoic membrane (Tagaya et al., 1961; Kitamura et al., 1967; Ishii et al., 2002). The DIs-derived recombinant viruses express high levels of viral and inserted genes, even in non-permissive cell lines without any cytopathic effects (Ishii et al., 2002). In earlier studies, MVA strain of vaccinia virus, which is also replication-incompetent in most mammal cells, was used to express a variety of foreign genes and some of these recombinant viruses were studied as candidate vaccine vectors and appeared to be more effective than many replication-competent vaccinia virus vaccines (Sutter and Moss, 1992; Sutter et al., 1994; Belyakov et al., 1998; Nam et al., 1999; Stittelaar et al., 2000). rDIs does not replicate nor produce infectious virions in most mammalian cells, therefore the DIs strain has a safety advantage when used as a recombinant vaccine vector as for MVA. Recently, a recombinant DIs, rDIsSIVGag, expressing a full-length *gag* gene of SIV, was developed, and demonstrated to have a potential for use as an HIV/AIDS vaccine (Someya et al., 2004).

Attempts at vaccine development against SARS-CoV are ongoing by a number of organizations using various techniques (see review, (Groneberg et al., 2005)). DNA vaccines (Kim et al., 2004; Yang et al., 2004; Zhu et al., 2004; Zhao et al., 2005) and viral vectors such as vaccinia virus (Bisht et al., 2004; Weingartl et al., 2004), parainfluenza virus (Bukreyev et al., 2004), adenovirus (Zakhartchouk et al., 2005) and rhabdoviruses (Faber et al., 2005; Kapadia et al., 2005) are used as recombinant vaccines. Yang et al. (2004) showed that viral replication was reduced by more than six orders of magnitude in the lungs of mice vaccinated with these S plasmid DNA expression vectors, and protection was mediated by a humoral but not a T-cell-dependent immune mechanism. Bisht et al. (2004) showed that inoculation of BALB/c mice with a

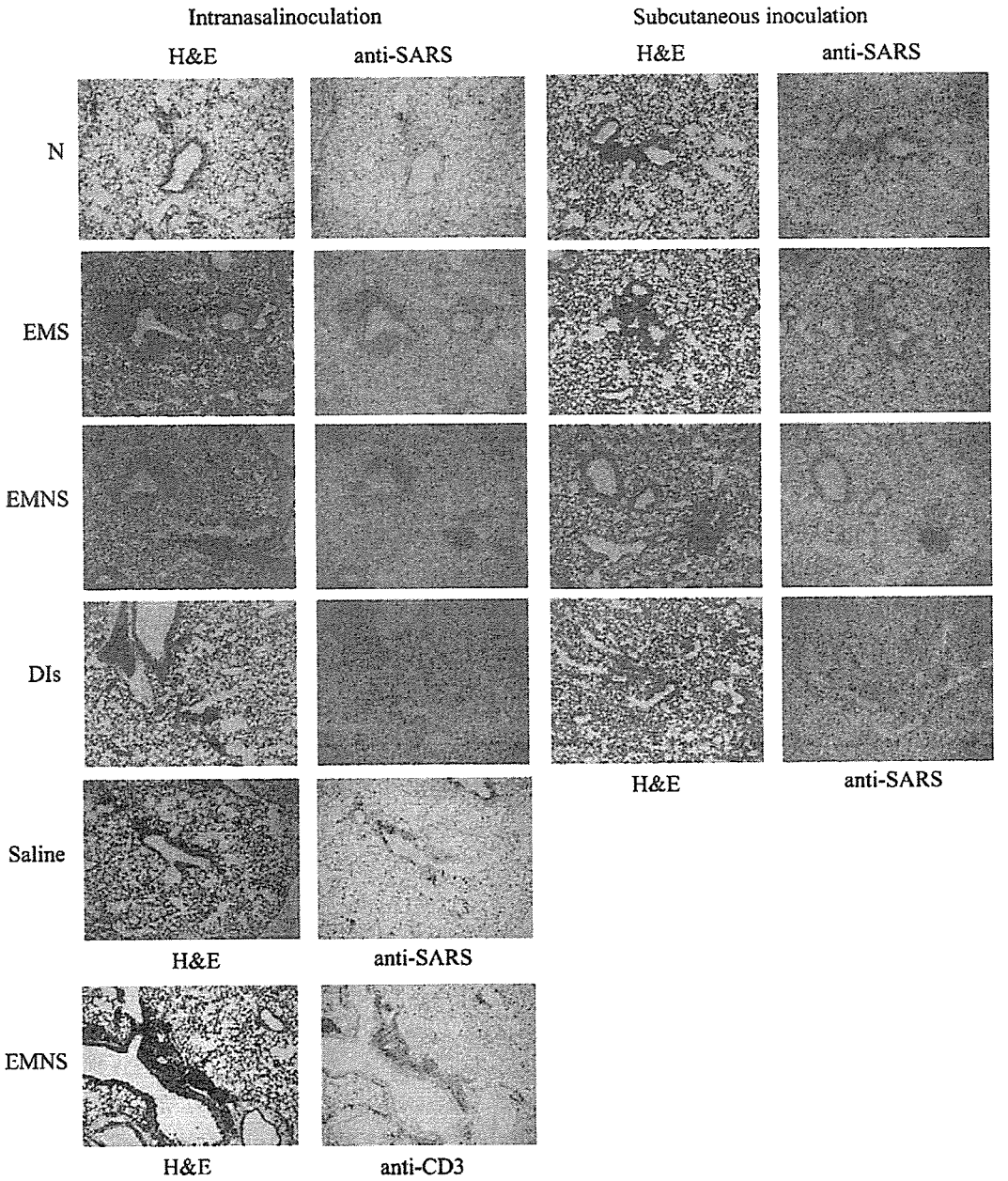

Fig. 8. Histopathology and immunohistochemistry. Lung specimen of mice immunized with rDIs expressing structural proteins of SARS-CoV and challenged with SARS-CoV. Mice were immunized i.n. or s.c. with DIs, rDIsSARS-N, rDIsSARS-E/M/S, rDIsSARS-E/M/N/S or saline. Mice were challenged with SARS-CoV 2 weeks after the final vaccination. Lungs were harvested 3 days after the challenge. The section was stained with hematoxylin and eosin (H&E) or immunohistochmically stained with anti-SARS-CoV antibody or anti-CD3 antibody.

recombinant MVA expressing SARS-CoV S protein elicited serum antibodies to SARS-CoV S protein and protective immunity against SARS-CoV infection. Previous studies demonstrated passive transfer of serum from immunized mice conferred protection against SARS-CoV in the respiratory tract following inoculation with either SARS CoV or recombinant MVA expressing S protein (Bisht et al., 2004; Subbarao et al., 2004). These results suggest that S protein is a crucial antigen in generating protective immunity. We observed that intranasal or subcutaneous inoculation of BALB/c mice with rDIs expressing S protein (rDIsSARS-S, rDIsSARS-E/M/S or rDIsSARS-E/M/N/S) produced serum antibodies capable of recognizing the SARS-CoV virion by ELISA, also capable of neutralizing SARS-CoV in vitro. The subcutaneous route appears to elicit stronger immunity than intranasal immunization with respect to the level of anti-SARS-CoV IgG antibody produced. Important finding here is that although the mucosal IgA antibody response was induced only in mice intranasally immunized with rDIsSARS-E/M/N/S, the mice administered with rDIsSARS-E/M/N/S by either route elicited strong protective immunity. Therefore, the protection was achieved in the absence of a mucosal IgA response in mice subcutaneously immunized with rDIsSARS-E/M/N/S. Thus, our results clearly show that mucosal infection might be prevented in the presence of a

high level of neutralizing serum IgG antibody. Control mice vaccinated with DIs not expressing envelope proteins were not protected, indicating that the effect was specific for the expressed envelope proteins of SARS-CoV and was not due to enhanced nonspecific immunity.

A recent report suggests that a combination of three adenovirus vector expressing SARS-S, -M and –N protein is capable of eliciting neutralizing antibodies in serum and N-specific T cell responses in rhesus macaques (Gao et al., 2003). However, in this report, the relationship between these immune responses and actual protection was not presented. In another study, the importance of SARS-CoV structural proteins in generating protective immunity was investigated by expressing them individually and in combination using a recombinant parainfluenza virus (PIV) type 3 vector. The expression of S with the two other putative virion envelope proteins, M and E protein, did not augment the neutralizing antibody response. In the absence of S, expression of M and E, or the nucleocapsid protein N, did not induce a detectable serum SARS-CoV-neutralizing antibody response (Buchholz et al., 2004). Our results were consistent with this in that expression of M or N proteins by administration of DIs harboring SARS-CoV M or N gene singly did not induce a neutralizing antibody response, although anti-SARS-CoV antibodies were detected by ELISA.

Recent studies have shown that vaccination with a plasmid expressing N protein can elicit SARS-CoV nucleocapsid-specific humoral and cellular immune responses (Kim et al., 2004; Zhu et al., 2004; Zhao et al., 2005). They showed that linkage of N protein to calreticulin, Ca^{2+}-binding protein known to enhance immune response, in a DNA vaccine resulted in the significant enhancement of the humoral and cellular immune responses to N protein in vaccinated mice. They also showed that the N protein-specific DNA vaccine elicited partial protection against N protein expressing vaccinia virus challenge, however, the efficacy of N-specific cellular immune responses in protection of SARS-CoV infection is not clear. Although we here showed that N protein expression by rDIs was capable of eliciting N-specific humoral and cellular immunity, vaccination with rDIsSARS-N failed to elicit a neutralizing antibody response against SARS-CoV infection in vitro, and failed to confer full protection in vaccinated mice against SARS-CoV challenge, suggesting that SARS-CoV N protein-specific antibodies and CTLs were not sufficient to provide full protection against SARS-CoV infection.

Histopathological analysis of lung tissues in the present study revealed a marked lymphocytic infiltration in peribronchial sites in mice immunized intranasally or subcutaneously with recombinant vaccinia virus DIs expressing E/M/S or E/M/N/S. Almost no SARS-CoV antigens were detected in these areas upon immunohistochemical analysis. The infiltrating lymphocytes were shown to be CD3 positive T-cells. This is the first evidence of induction of protective immunity against SARS-CoV associated with marked infiltration of T cells at a SARS-CoV infection site. We were able to detect SARS-CoV S-specific $CD8^+$ T cells in the spleen of these immunized mice by INF-γ ELISPOT. Thus, these results suggest that T cell induction in mice immunized with rDIsSARS-E/M/S and rDIsSARS-E/M/N/S might provide additional help to completely eliminate SARS-CoV in the lung. Of note, Weingartl et al. (2004) reported a low level of neutralizing antibody response in ferrets (*Mustela putorius furo*) immunized with a recombinant MVA expressing SARS-CoV S protein. They also showed that there are more rapid and vigorous neutralizing antibody responses in immunized ferrets, compared to control animals after challenge with SARS-CoV. However, SARS-CoV infection and spreading in the immunized ferrets is not prevented. Moreover, upon infection with SARS-CoV, strong inflammatory responses were noted in ferrets immunized with either recombinant MVA expressing SARS-CoV S or N protein, suggesting that vaccination with the recombinant MVA expressing SARS-CoV S or N protein may, in some case, lead to enhanced pathology during SARS-CoV infection (Czub et al., 2005; Weingartl et al., 2004). It was also reported that antibodies that neutralized most human SARS-CoV S enhanced entry mediated by the civet virus S, suggesting the possibility that such kind of vaccines might enhance viral infection (Yang et al., 2005). Although we observed no such pathology in rDIs-immunized mice after virus challenge, the potential for widespread tissue damage following administration of SARS-CoV proteins should be carefully investigated. In addition, further studies are required to clarify whether the recruited T-cells indeed play an important role in clearance of SARS-CoV from sites of infection.

In this study, we constructed rDIs containing genes encoding four structural proteins of SARS-CoV that were individually or simultaneously expressed. Intranasal or subcutaneous inoculation of BALB/c 3T3 mice with rDIs expressing S protein with or without other structural proteins elicited a high level of neutralizing antibodies against SARS-CoV and protective immunity, in the lungs of mice after intranasal challenge. Furthermore, both cellular and mucosal immunity against SARS-CoV structural proteins were also induced following administration of the rDIs. Therefore, the replication-deficient DIs strain is a feasible, safe and effective SARS vaccine vector.

Materials and methods

Cells

CEF cells and Vero E6 cells were grown in Dulbecco's modified essential medium (DMEM) supplemented with 10% fetal bovine serum (FCS), 1% penicillin-streptomycin and L-glutamine (GIBCO BRL/Life Technologies, Gaithersburg, MD). A20.2J murine B cells were maintained in RPMI1640 supplemented with 10% FCS, 50 μM β-mercaptoethanol, L-glutamine and antibiotics.

Plasmid DNA constructs and DNA preparation

cDNA encoding SARS-CoV structural proteins were generated by reverse transcription of SARS-CoV HKU39849

(Accession No. AY278491) using superscriptII (Invitrogen Corp., Carlsbad, CA), followed by amplification using expand high fidelity PCR system (Roche diagnostics), as described previously (Ohnishi et al., 2005). These DNA fragments encoding E, M, N and S proteins were cloned into the vaccinia virus transfer vector pDIsgptmH5, which also harbored E. coli xanthine-guanine phosphoribosyltransferase, under control of a vaccinia virus p7.5 promoter in the cloning site of pUc/DIs (Ishii et al., 2002), to generate pDIsSARS-E, pDIsSARS-M, pDIsSARS-N, and pDIsSARS-S, respectively. To construct transfer vectors to generate rDIs expressing E/M, E/M/S, or E/M/N/S, DNA fragments encoding M, N and S proteins controlled by the mH5 promoter of the vaccinia virus (Wyatt et al., 1996) were inserted into pDIsSARS-E *Sma*I, *Not*I and *Sac*I sites, respectively, thus generating pDIsSARS-E/M, pDIsSARS-E/M/S and pDIsSARS-E/M/N/S (Fig. 1). A plasmid expressing S driven by the EF-1α promoter was constructed using pEF-BOS-bst (Yoshizawa et al., 2001), and designated pEF-S-bst.

Generation of recombinant vaccinia virus

Recombinant forms of DIs were obtained by hypoxanthine-guanine phosphoribosyltransferase selection (Falkner and Moss, 1988). Monolayers of CEF cells in 6-well plates were pre-incubated with DMEM containing 10% FCS, 25 μg/ml of micophenoic acid (MPA), 250 μg/ml of xanthine and 15 μg/ml of hypoxanthine. Infection was performed onto CEF cells grown in 8 cm dishes with DIs at a multiplicity of infection (moi) of 1.0. Transfection was performed using 20 μg of each DIs transfer vector and Lipofectamine (GIBCO BRL/Life Technologies). rDIs expressing SARS-CoV structural proteins were selected following four consecutive rounds of plaque purification of CEF cells in 6-well plates pre-incubated with DMEM containing 10% FCS, 25 μg/ml of MPA, 250 μg/ml of xanthine, and 15 μg/ml of hypoxanthine. Resultant rDIs expressing SARS-CoV structural proteins were designated as rDIsSARS-E, rDIsSARS-M, rDIsSARS-N, rDIsSARS-S, rDIsSARS-E/M, rDIsSARS-E/M/S and rDIsSARS-E/M/N/S, respectively, and subsequently maintained in CEF cells for use in further studies.

Western blot analysis

CEF cells infected with rDIs constructs harboring ORFs of SARS-CoV structural proteins were fractionated by SDS-PAGE under reduced conditions. Purified SARS-CoV virion (0.5 μg) was used as a positive control. The proteins were then transferred to an Immobilon-P PVDF membrane (MILLIPORE, Bedford, MA) and incubated with monoclonal antibodies against N or S proteins (Ohnishi et al., 2005) or polyclonal antibody against M protein (Mizutani et al., 2004). After washing, the membrane was reacted with HRP-conjugated Fab fragment of anti-mouse or rabbit IgG (H + L) (1:20,000, Santa Cruz Biotechnology, Santa Cruz, CA), followed by visualization of the bands using chemiluminescent reagents (Pierce, Rockford, IL).

Indirect immunofluorescence analysis

CEF cells were infected with rDIs expressing SARS-CoV structural proteins. After 48 h of incubation, the cells were washed with PBS and fixed with 3% paraformaldehyde in PBS for 20 min at room temperature. The fixed cells were then permeabilized with 0.2% Triton X-100 for 3 min at room temperature, and then blocked with a non-fat milk solution, Block Ace (Yukijirushi Co., Tokyo, Japan). The cells were incubated with polyclonal antibodies against M, N or S proteins (Mizutani et al., 2004) for 60 min at 37 °C. The cells were further incubated with fluorescein isothiocyanate (FITC)-conjugated goat anti-rabbit IgG (TAGO, Burlingame, CA) diluted to 1:500 in PBS to detect SARS-CoV M, N or S proteins. To analyze the subcellular localization of SARS structural proteins, anti-GM-130 monoclonal antibody (BD Biosciences, Mississauga, ON, Canada) and rhodamine-conjugated goat anti-mouse IgG (TAGO) were used to stain the Golgi apparatus.

Vaccination

Animal studies were carried out under a protocol approved by the Animal Care and Use Committee of the National Institute of Infectious Diseases, Japan. Five- to 6-week-old female BALB/c mice were purchased from Japan SLC (Hamamatsu, Japan) and immunized with 10^6 pfu of rDIs, either subcutaneously (s.c.) or intranasally (i.n.). After 2 and 6 weeks, identical titers of recombinant virus were re-administered. One week later, the mice were intranasally challenged with 10^4 $TCID_{50}$ of SARS-CoV in 20 μl of saline as previously described (Subbarao et al., 2004). Three days later, serum, nasal wash fluid and bronchoalveolar wash fluid were collected to measure viral titers and antibodies against SARS-CoV from mice that were sacrificed under anesthesia with chloroform.

Detection of SARS-CoV specific IgA and IgG antibodies

IgA and IgG titers against SARS-CoV were determined by ELISA, as previously described (Takasuka et al., 2004). Briefly, microtiter plates (Dynatech, Chantily, VA) were coated overnight at 4 °C with SARS-CoV-infected or mock-infected Vero E6 cell lysate samples previously treated with 1% NP40, followed by UV-inactivation. The plates were blocked with 1% OVA in PBS–0.05% Tween 20, and then incubated with serially diluted sera (1:10–$1:25^5$) for 1 h at room temperature. The plates were then incubated with either peroxidase-conjugated anti-mouse IgG (1:2000, Zymed, South San Francisco, CA) or IgA (1:2000, Southern Biotechnology, Birmingham, AL) antibody. The plates were washed three times with PBS-Tween at each step. The substrate mixture (o-phenylenediamine (Zymed) and hydrogen peroxide) was added to each well, and the absorbance of each well was read at 490 nm using a model 680 microplate reader (Bio-Rad, Hercules, CA). To provide a standard for IgG detection, serum was obtained from a hyper-immunized mouse and the OD490nm value of 100 ELISA units/ml of standard serum was around three in every assay.

Each SARS-CoV-specific IgG titer was calculated by subtracting the optical density of wells coated with non-infected cell lysate from the optical density of wells coated with virus-infected cell lysate. As a positive control to induce SARS-CoV-specific IgA, mice were immunized intranasally with UV-inactivated purified SARS-CoV together with 3 μg of poly(I:C) (Ichinohe et al., 2005).

SARS-CoV neutralizing assay

Sera collected from vaccinated mice were inactivated by incubation at 56 °C for 30 min. The serially diluted mice sera (up to five-fold) were incubated with 100 $TCID_{50}$ of SARS-CoV for 1 h, then the mixtures were added to a Vero E6 cell culture grown to confluence in 96-well microtiter plates. After 48 h, the cells were fixed with 10% formaldehyde and stained with crystal violet to visualize the cytopathic effects of the virus (Storch, 2001). Neutralization antibody titers were expressed as the minimal dilution of sera capable of inhibiting viral cytopathic effects.

Analysis of the SARS-CoV-specific T-cell response

CLN, ALN and spleens were obtained from mice 1 week after their third vaccination. Following preparation of a single cell suspension, T cells were purified using a Pan T cell isolation kit and a magnetic cell sort system (MACS: Miltenyi Biotec, Bergisch Gladbach, Germany). To prepare APC, normal BALB/c mouse splenocytes were depleted of Thy-1^+ T cells by MACS and irradiated at 2000 cGy. Purified T cells (1×10^6) were cultured with APC (5×10^6) in the presence or absence of UV-irradiated, purified SARS-CoV virion at 10 μg/ml. Four days after cultivation, cytokine concentrations within culture supernatant were measured by flow cytometry using a mouse Th1/Th2 cytokine cytometric bead array kit (Becton Dickinson, San Jose, CA).

Generation of a stable S-transfectant

A20.2J murine B cells were transfected with either pEF-S-bst or pEF-BOS-bst by electroporation at 960 μF and 310 V using a GenePulser (BioRad Laboratories, Hercules, CA). After selection using blasticidine S (Invitrogen), followed by limiting dilution cloning, S6.2 and BOS-5 clones were obtained. To detect S protein expression in S6.2 cells, the cells were stained with biotinylated anti-S monoclonal antibody (Ohnishi et al., 2005) or control antibody, followed by the incubation with APC-streptavidin (e-Bioscience Inc., San Diego, CA), after which they were analyzed by FACScalibur (BD Bioscience) using the Cell Quest II program. Propidium Iodide was used to exclude dead cells. The data were re-analyzed and depicted using Flowjo software (Tree Star Inc., San Carlos, CA).

ELISPOT assay

Spleen T cells of mice immunized with rDIsSARS-N or rDIsSARS- E/M/N/S were separated using a MACS system (Miltenyi Biotec, Auburn, CA). To enrich $CD4^+$ T cells in the T cell fraction, $CD8^+$ T cells were partially removed using anti-CD8 mAb-coated magnetic beads (Miltenyi Biotec). This procedure reduced the number of $CD8^+$ T cells to less than one third. Overlapping 20-mer peptides covering the whole N sequences of SARS-CoV were obtained from Sigma-Aldrich Japan. S peptides S44 (S331–350), S45 (S381–400), S46 (S431–450), and S47 (S481–500) corresponding to the ACE2 binding region of the S protein were selectively produced based on a web-site program by SYFPEITHI (http://syfpeithi.de/). A20.2J murine B cells irradiated at 2000 cGy were used as APCs with peptides corresponding to either S or N proteins. In some experiments, A20.2J cells stably transfected with pEF-S or the empty vector pEF-BOS were used.

ELISPOT assays were performed according to the methods outlined by DIACLONE research (Besancon, France). In brief, 96-well flat-bottom plates (Maxisoap Nunc plates, Nunc, Rochester, NY) were coated with anti-IFN-γ capture antibody for one h at 37 °C. The plates were then washed with PBS containing 0.05% Tween 20 (PBST), and blocked with PBS containing 2% bovine serum albumin overnight at 4 °C. Freshly isolated splenic T cells (5×10^5) and APCs (1×10^4) were added to the plates in the presence or absence of 5 μM of N or S peptides and incubated for 16 h at 37 °C in 5% CO_2 on the anti-IFN-γ-coated plates, followed by a lysis with ice-cold deionized water. After the plates were washed, biotinylated detection antibody was added, then the plates were further incubated for 1 h at 37 °C. The plates were washed three times with PBST, then 50 μl/well of Streptavidin-alkaline phosphatase-conjugated anti-biotin immunoglobulin G solution was added, followed by incubation for 1 h at 37 °C. After washing with PBST, substrate mix (50 μl/well) was added, and the plates were allowed to develop over 4 h at 37 °C. The wells were imaged and the number of spot-forming cells SFC counted using a KS ELISPOT compact system (Carl Zeiss, Jena, Germany).

Histopathology and immunohistochemistry

Lung tissue from the mice was fixed in 10% buffered formalin and embedded in paraffin. Paraffin block sections were stained with hematoxylin and eosin (H&E). SARS-CoV antigens were immunohistochemically detected using a labeled-streptoavidin–biotin complex staining system (DakoCytomation Co. Japan, Kyoto, Japan). Rabbit polyclonal antibodies raised against UV-inactivated, purified SARS-CoV were used as a primary antibody. A catalyzed signal amplification method (Dako) was also used to detect SARS-CoV antigens with enhanced sensitivity. Lung sections from mice vaccinated with rDIsSARS-E/M/N/S and infected with SARS Co-V were stained with anti-CD3 antibody. (Santa Cruz Biotechnology)

Acknowledgments

We would like to thank Dr. Michinori Kohara for kindly providing us anti-SARS-CoV polyclonal antibodies. We would

also like to thank Ms. Mami Matsuda, Ms. Makiko Yahata, Ms. Sayaka Yoshizaki, Ms. Chikako Sato, Mr. Masayuki Ishige, Ms. Yuko Sato and Ms. Aya Harashima for their excellent technical support. This work was supported by a Heath and Labour Science Research Grant from the Ministry of Health, Labour, and Welfare, Japan, and from the New Energy and Industrial Technology Development Organization (NEDO) of Japan.

References

Anton, I.M., Gonzalez, S., Bullido, M.J., Corsin, M., Risco, C., Langeveld, J.P., Enjuanes, L., 1996. Cooperation between transmissible gastroenteritis coronavirus (TGEV) structural proteins in the in vitro induction of virus-specific antibodies. Virus Res. 46 (1–2), 111–124.

Belyakov, I.M., Wyatt, L.S., Ahlers, J.D., Earl, P., Pendleton, C.D., Kelsall, B.L., Strober, W., Moss, B., Berzofsky, J.A., 1998. Induction of a mucosal cytotoxic T-lymphocyte response by intrarectal immunization with a replication-deficient recombinant vaccinia virus expressing human immunodeficiency virus 89.6 envelope protein. J. Virol. 72, 8264–8272.

Bisht, H., Roberts, A., Vogel, L., Bukreyev, A., Collins, P.L., Murphy, B.R., Subbarao, K., Moss, B., 2004. Severe acute respiratory syndrome coronavirus spike protein expressed by attenuated vaccinia virus protectively immunizes mice. Proc. Natl. Acad. Sci. U. S. A. 101 (17), 6641–6646.

Buchholz, U.J., Bukreyev, A., Yang, L., Lamirande, E.W., Murphy, B.R., Subbarao, K., Collins, P.L., 2004. Contributions of the structural proteins of severe acute respiratory syndrome coronavirus to protective immunity. Proc. Natl. Acad. Sci. U. S. A. 101 (26), 9804–9809.

Bukreyev, A., Lamirande, E.W., Buchholz, U.J., Vogel, L.N., Elkins, W.R., St Claire, M., Murphy, B.R., Subbarao, K., Collins, P.L., 2004. Mucosal immunisation of African green monkeys (*Cercopithecus aethiops*) with an attenuated parainfluenza virus expressing the SARS coronavirus spike protein for the prevention of SARS. Lancet 363 (9427), 2122–2127.

Collins, A.R., Knobler, R.L., Powell, H., Buchmeier, M.J., 1982. Monoclonal antibodies to murine hepatitis virus-4 (strain JHM) define the viral glycoprotein responsible for attachment and cell–cell fusion. Virology 119 (2), 358–371.

Collisson, E.W., Pei, J., Dzielawa, J., Seo, S.H., 2000. Cytotoxic T lymphocytes are critical in the control of infectious bronchitis virus in poultry. Dev. Comp. Immunol. 24 (2–3), 187–200.

Czub, M., Weingartl, H., Czub, S., He, R., Cao, J., 2005. Evaluation of modified vaccinia virus Ankara based recombinant SARS vaccine in ferrets. Vaccine 23 (17–18), 2273–227 9.

Drosten, C., Gunther, S., Preiser, W., van der Werf, S., Brodt, H.R., Becker, S., Rabenau, H., Panning, M., Kolesnikova, L., Fouchier, R.A., Berger, A., Burguiere, A.M., Cinatl, J., Eickmann, M., Escriou, N., Grywna, K., Kramme, S., Manuguerra, J.C., Muller, S., Rickerts, V., Sturmer, M., Vieth, S., Klenk, H.D., Osterhaus, A.D., Schmitz, H., Doerr, H.W., 2003. Identification of a novel coronavirus in patients with severe acute respiratory syndrome. N. Engl. J. Med. 348 (20), 1967–1976.

Faber, M., Lamirande, E.W., Roberts, A., Rice, A.B., Koprowski, H., Dietzschold, B., Schnell, M.J., 2005. A single immunization with a rhabdovirus-based vector expressing severe acute respiratory syndrome coronavirus (SARS-CoV) S protein results in the production of high levels of SARS-CoV-neutralizing antibodies. J. Gen. Virol. 86 (Pt. 5), 1435–1440.

Falkner, F.G., Moss, B., 1988. *Escherichia coli* gpt gene provides dominant selection for vaccinia virus open reading frame expression vectors. J. Virol. 62 (6), 1849–1854.

Fouchier, R.A., Kuiken, T., Schutten, M., van Amerongen, G., van Doornum, G.J., van den Hoogen, B.G., Peiris, M., Lim, W., Stohr, K., Osterhaus, A.D., 2003. Aetiology: Koch's postulates fulfilled for SARS virus. Nature 423 (6937), 240.

Gao, W., Tamin, A., Soloff, A., D'Aiuto, L., Nwanegbo, E., Robbins, P.D., Bellini, W.J., Barratt-Boyes, S., Gambotto, A., 2003. Effects of a SARS-associated coronavirus vaccine in monkeys. Lancet 362 (9399), 1895–1896.

Groneberg, D.A., Poutanen, S.M., Low, D.E., Lode, H., Welte, T., Zabel, P., 2005. Treatment and vaccines for severe acute respiratory syndrome. Lancet, Infect. Dis. 5 (3), 147–155.

Holmes, K.V., 2003. SARS coronavirus: a new challenge for prevention and therapy. J. Clin. Invest. 111 (11), 1605–1609.

Ichinohe, T., Watanabe, I., Ito, S., Fujii, H., Moriyama, M., Tamura, S., Takahashi, H., Sawa, H., Chiba, J., Kurata, T., Sata, T., Hasegawa, H., 2005. Synthetic double-stranded RNA poly (I:C) combined with mucosal vaccine protects against influenza virus infection. J. Virol. 79 (5), 2910–2919.

Ishii, K., Ueda, Y., Matsuo, K., Matsuura, Y., Kitamura, T., Kato, K., Izumi, Y., Someya, K., Ohsu, T., Honda, M., Miyamura, T., 2002. Structural analysis of vaccinia virus DIs strain: application as a new replication-deficient viral vector. Virology 302 (2), 433–444.

Jackwood, M.W., Hilt, D.A., 1995. Production and immunogenicity of multiple antigenic peptide (MAP) constructs derived from the S1 glycoprotein of infectious bronchitis virus (IBV. Adv. Exp. Med. Biol. 380, 213–219.

Kapadia, S.U., Rose, J.K., Lamirande, E., Vogel, L., Subbarao, K., Roberts, A., 2005. Long-term protection from SARS coronavirus infection conferred by a single immunization with an attenuated VSV-based vaccine. Virology 340, 174–182.

Kim, T.W., Lee, J.H., Hung, C.F., Peng, S., Roden, R., Wang, M.C., Viscidi, R., Tsai, Y.C., He, L., Chen, P.J., Boyd, D.A., Wu, T.C., 2004. Generation and characterization of DNA vaccines targeting the nucleocapsid protein of severe acute respiratory syndrome coronavirus. J. Virol. 78 (9), 4638–4645.

Kitamura, T., Kitamura, T., Tagaya, I., 1967. Immunogenicity of an attenuated strain of vaccinia virus on rabbits and monkeys. Nature 215, 1187–1188.

Ksiazek, T.G., Erdman, D., Goldsmith, C.S., Zaki, S.R., Peret, T., Emery, S., Tong, S., Urbani, C., Comer, J.A., Lim, W., Rollin, P.E., Dowell, S.F., Ling, A.E., Humphrey, C.D., Shieh, W.J., Guarner, J., Paddock, C.D., Rota, P., Fields, B., DeRisi, J., Yang, J.Y., Cox, N., Hughes, J.M., LeDuc, J.W., Bellini, W.J., Anderson, L.J., 2003. A novel coronavirus associated with severe acute respiratory syndrome. N. Engl. J. Med. 348 (20), 1953–1966.

Li, W., Moore, M.J., Vasilieva, N., Sui, J., Wong, S.K., Berne, M.A., Somasundaran, M., Sullivan, J.L., Luzuriaga, K., Greenough, T.C., Choe, H., Farzan, M., 2003. Angiotensin-converting enzyme 2 is a functional receptor for the SARS coronavirus. Nature 426 (6965), 450–454.

Marra, M.A., Jones, S.J., Astell, C.R., Holt, R.A., Brooks-Wilson, A., Butterfield, Y.S., Khattra, J., Asano, J.K., Barber, S.A., Chan, S.Y., Cloutier, A., Coughlin, S.M., Freeman, D., Gim, N., Griffith, O.L., Leach, S.R., Mayo, M., McDonald, H., Montgomery, S.B., Pandoh, P.K., Petrescu, A.S., Robertson, A.G., Schein, J.E., Siddiqui, A., Smailus, D.E., Stott, J.M., Yang, G.S., Plummer, F., Andonov, A., Artsob, H., Bastien, N., Bernard, K., Booth, T.F., Bowness, D., Czub, M., Drebot, M., Fernando, L., Flick, R., Garbutt, M., Gray, M., Grolla, A., Jones, S., Feldmann, H., Meyers, A., Kabani, A., Li, Y., Normand, S., Stroher, U., Tipples, G.A., Tyler, S., Vogrig, R., Ward, D., Watson, B., Brunham, R.C., Krajden, M., Petric, M., Skowronski, D.M., Upton, C., Roper, R.L., 2003. The Genome sequence of the SARS-associated coronavirus. Science 300 (5624), 1399–1404.

Meeusen, E.N., Scheerlinck, J.P., Wattegedera, S., Entrican, G., 2004. Advances in mucosal vaccination. Anim. Health Res. Rev. 5 (2), 209–217.

Mizutani, T., Fukushi, S., Saijo, M., Kurane, I., Morikawa, S., 2004. Phosphorylation of p38 MAPK and its downstream targets in SARS coronavirus-infected cells. Biochem. Biophys. Res. Commun. 319 (4), 1228–1234.

Nal, B., Chan, C., Kien, F., Siu, L., Tse, J., Chu, K., Kam, J., Staropoli, I., Crescenzo-Chaigne, B., Escriou, N., van der Werf, S., Yuen, K.Y., Altmeyer, R., 2005. Differential maturation and subcellular localization of severe acute respiratory syndrome coronavirus surface proteins S, M and E. J. Gen. Virol. 86 (Pt. 5), 1423–1434.

Nam, J.H., Wyatt, L.S., Chae, S.L., Cho, H.W., Park, Y.K., Moss, B., 1999. Protection against lethal Japanese encephalitis virus infection of mice by immunization with the highly attenuated MVA strain of vaccinia virus expressing JEV prM and E genes. Vaccine 17 (3), 261–268.

Ohnishi, K., Sakaguchi, M., Kaji, T., Akagawa, K., Taniyama, T., Kasai, M., Tsunetsugu-Yokota, Y., Oshima, M., Yamamoto, K., Takasuka, N., Hashimoto, S., Ato, M., Fujii, H., Takahashi, Y., Morikawa, S., Ishii, K., Sata, T., Takagi, H., Itamura, S., Odagiri, T., Miyamura, T., Kurane, I., Tashiro, M., Kurata, T., Yoshikura, H., Takemori, T., 2005. Immunological

detection of severe acute respiratory syndrome coronavirus by monoclonal antibodies. Jpn. J. Infect. Dis. 58 (2), 88–94.

Peiris, J.S., Lai, S.T., Poon, L.L., Guan, Y., Yam, L.Y., Lim, W., Nicholls, J., Yee, W.K., Yan, W.W., Cheung, M.T., Cheng, V.C., Chan, K.H., Tsang, D.N., Yung, R.W., Ng, T.K., Yuen, K.Y., 2003. Coronavirus as a possible cause of severe acute respiratory syndrome. Lancet 361 (9366), 1319–1325.

Rota, P.A., Oberste, M.S., Monroe, S.S., Nix, W.A., Campagnoli, R., Icenogle, J.P., Penaranda, S., Bankamp, B., Maher, K., Chen, M.H., Tong, S., Tamin, A., Lowe, L., Frace, M., DeRisi, J.L., Chen, Q., Wang, D., Erdman, D.D., Peret, T.C., Burns, C., Ksiazek, T.G., Rollin, P.E., Sanchez, A., Liffick, S., Holloway, B., Limor, J., McCaustland, K., Olsen-Rasmussen, M., Fouchier, R., Gunther, S., Osterhaus, A.D., Drosten, C., Pallansch, M.A., Anderson, L.J., Bellini, W.J., 2003. Characterization of a novel coronavirus associated with severe acute respiratory syndrome. Science 300 (5624), 1394–1399.

Ruan, Y.J., Wei, C.L., Ee, A.L., Vega, V.B., Thoreau, H., Su, S.T., Chia, J.M., Ng, P., Chiu, K.P., Lim, L., Zhang, T., Peng, C.K., Lin, E.O., Lee, N.M., Yee, S.L., Ng, L.F., Chee, R.E., Stanton, L.W., Long, P.M., Liu, E.T., 2003. Comparative full-length genome sequence analysis of 14 SARS coronavirus isolates and common mutations associated with putative origins of infection. Lancet 361 (9371), 1779–1785.

Seo, S.H., Wang, L., Smith, R., Collisson, E.W., 1997. The carboxyl-terminal 120-residue polypeptide of infectious bronchitis virus nucleocapsid induces cytotoxic T lymphocytes and protects chickens from acute infection. J. Virol. 71 (10), 7889–7894.

Someya, K., Xin, K.Q., Matsuo, K., Okuda, K., Yamamoto, N., Honda, M., 2004. A consecutive priming-boosting vaccination of mice with simian immunodeficiency virus (SIV) gag/pol DNA and recombinant vaccinia virus strain DIs elicits effective anti-SIV immunity. J. Virol. 78 (18), 9842–9853.

Stittelaar, K.J., Wyatt, L.S., de Swart, R.L., Vos, H.W., Groen, J., van Amerongen, G., van Binnendijk, R.S., Rozenblatt, S., Moss, B., Osterhaus, A.D., 2000. Protective immunity in macaques vaccinated with a modified vaccinia virus Ankara-based measles virus vaccine in the presence of passively acquired antibodies. J. Virol. 74, 4236–4243.

Storch, G.A., 2001. Diagnostic virology. In: David, P.M.H., Knipe, M. (Eds.), Fields Virology, 4th ed. Lippincott Williams & Wilkins, Philadelphia, PA, pp. 493–531.

Subbarao, K., McAuliffe, J., Vogel, L., Fahle, G., Fischer, S., Tatti, K., Packard, M., Shieh, W.J., Zaki, S., Murphy, B., 2004. Prior infection and passive transfer of neutralizing antibody prevent replication of severe acute respiratory syndrome coronavirus in the respiratory tract of mice. J. Virol. 78 (7), 3572–3577.

Sutter, G., Moss, B., 1992. Nonreplicating vaccinia vector efficiently expresses recombinant genes. Proc. Natl. Acad. Sci. U. S. A. 89, 10847–10851.

Sutter, G., Wyatt, L.S., Foley, P.L., Bennink, J.R., Moss, B., 1994. A recombinant vector derived from the host range-restricted and highly attenuated MVA strain of vaccinia virus stimulates protective immunity in mice to influenza virus. Vaccine 12, 1032–1040.

Tagaya, I., Kitamura, T., Sano, Y., 1961. A new mutant of dermovaccinia virus. Nature 192, 381–382.

Takasuka, N., Fujii, H., Takahashi, Y., Kasai, M., Morikawa, S., Itamura, S., Ishii, K., Sakaguchi, M., Ohnishi, K., Ohshima, M., Hashimoto, S., Odagiri, T., Tashiro, M., Yoshikura, H., Takemori, T., Tsunetsugu-Yokota, Y., 2004. A subcutaneously injected UV-inactivated SARS coronavirus vaccine elicits systemic humoral immunity in mice. Int. Immunol. 16 (10), 1423–1430.

Weingartl, H., Czub, M., Czub, S., Neufeld, J., Marszal, P., Gren, J., Smith, G., Jones, S., Proulx, R., Deschambault, Y., Grudeski, E., Andonov, A., He, R., Li, Y., Copps, J., Grolla, A., Dick, D., Berry, J., Ganske, S., Manning, L., Cao, J., 2004. Immunization with modified vaccinia virus Ankara-based recombinant vaccine against severe acute respiratory syndrome is associated with enhanced hepatitis in ferrets. J. Virol. 78 (22), 12672–12676.

Weisz, O.A., Swift, A.M., Machamer, C.E., 1993. Oligomerization of a membrane protein correlates with its retention in the Golgi complex. J. Cell Biol. 122 (6), 1185–1196.

Wyatt, L.S., Shors, S.T., Murphy, B.R., Moss, B., 1996. Development of a replication-deficient recombinant vaccinia virus vaccine effective against parainfluenza virus 3 infection in an animal model. Vaccine 14 (15), 1451–1458.

Xiao, X., Chakraborti, S., Dimitrov, A.S., Gramatikoff, K., Dimitrov, D.S., 2003. The SARS-CoV S glycoprotein: expression and functional characterization. Biochem. Biophys. Res. Commun. 312 (4), 1159–11564.

Yang, Z.Y., Kong, W.P., Huang, Y., Roberts, A., Murphy, B.R., Subbarao, K., Nabel, G.J., 2004. A DNA vaccine induces SARS coronavirus neutralization and protective immunity in mice. Nature 428 (6982), 561–564.

Yang, Z.Y., Werner, H.C., Kong, W.P., Leung, K., Traggiai, E., Lanzavecchia, A., Nabel, G.J., 2005. Evasion of antibody neutralization in emerging severe acute respiratory syndrome coronaviruses. Proc. Natl. Acad. Sci. U. S. A. 102 (3), 797–801.

Yoshizawa, I., Soda, Y., Mizuochi, T., Yasuda, S., Rizvi, T.A., Takemori, T., Tsunetsugu-Yokota, Y., 2001. Enhancement of mucosal immune response against HIV-1 Gag by DNA immunization. Vaccine 19 (20–22), 2995–3003.

You, J., Dove, B.K., Enjuanes, L., DeDiego, M.L., Alvarez, E., Howell, G., Heinen, P., Zambon, M., Hiscox, J.A., 2005. Subcellular localization of the severe acute respiratory syndrome coronavirus nucleocapsid protein. J. Gen. Virol. 86 (Pt. 12), 3303–3310.

Zakhartchouk, A.N., Viswanathan, S., Mahony, J.B., Gauldie, J., Babiuk, L.A., 2005. Severe acute respiratory syndrome coronavirus nucleocapsid protein expressed by an adenovirus vector is phosphorylated and immunogenic in mice. J. Gen. Virol. 86 (Pt. 1), 211–215.

Zhao, P., Cao, J., Zhao, L.J., Qin, Z.L., Ke, J.S., Pan, W., Ren, H., Yu, J.G., Qi, Z.T., 2005. Immune responses against SARS-coronavirus nucleocapsid protein induced by DNA vaccine. Virology 331 (1), 128–135.

Zhi, Y., Kobinger, G.P., Jordan, H., Suchma, K., Weiss, S.R., Shen, H., Schumer, G., Gao, G., Boyer, J.L., Crystal, R.G., Wilson, J.M., 2005. Identification of murine CD8 T cell epitopes in codon-optimized SARS-associated coronavirus spike protein. Virology 335 (1), 34–45.

Zhu, M.S., Pan, Y., Chen, H.Q., Shen, Y., Wang, X.C., Sun, Y.J., Tao, K.H., 2004. Induction of SARS-nucleoprotein-specific immune response by use of DNA vaccine. Immunol. Lett. 92 (3), 237–243.

Inhibition of cell proliferation by SARS-CoV infection in Vero E6 cells

Tetsuya Mizutani[1], Shuetsu Fukushi[1], Daisuke Iizuka[2], Osamu Inanami[2], Mikinori Kuwabara[2], Hideaki Takashima[3], Hiroshi Yanagawa[3], Masayuki Saijo[1], Ichiro Kurane[1] & Shigeru Morikawa[1]

[1]Special Pathogens Laboratory, Department of Virology 1, National Institute of Infectious Diseases, Tokyo, Japan; [2]Laboratory of Radiation Biology, Department of Environmental Veterinary Sciences, Graduate School of Veterinary Medicine, Hokkaido University, Sapporo, Japan; and [3]Department of Biosciences and Informatics, Faculty of Science and Technology, Keio University, Yokohama, Japan

Correspondence: Tetsuya Mizutani, Special Pathogens Laboratory, Department of Virology 1, National Institute of Infectious Diseases, Gakuen 4-7-1, Musashimurayama, Tokyo 208-0011, Japan. Tel.: + 81 42 561 0771; fax: + 81 42 564 4881; e-mail: tmizutan@nih.go.jp

Received 21 June 2005; revised 15 August 2005; accepted 13 September 2005.
First published online 16 November 2005.

doi:10.1111/j.1574-695X.2005.00028.x

Editor: Alex van Belkum

Keywords
SARS-CoV; cell proliferation; PI3K/Akt; GSK-3β; apoptosis.

Abstract

Severe acute respiratory syndrome (SARS) is caused by SARS-coronavirus (SARS-CoV). Infection of Vero E6 cells with SARS-CoV inhibits cell proliferation. Our previous study indicated that Akt, which is poorly phosphorylated in confluent cultures of Vero E6 cells, is phosphorylated and then dephosphorylated upon infection by SARS-CoV. In the present study, we showed that a serine residue of Akt was phosphorylated in Vero E6 cells in subconfluent culture and that Akt was dephosphorylated rapidly after SARS-CoV infection without up-regulation of its phosphorylation. Phosphorylation of glycogen synthase kinase-3β, which is one of the downstream targets of Akt, was prevented in SARS-CoV-infected cells. However, treatment with glycogen synthase kinase-3β small interfering RNA indicated that the glycogen synthase kinase-3β signaling pathway was not related to inhibition of cell proliferation. Treatment of Vero E6 cells with the phosphatidylinositol 3′-kinase/Akt inhibitor, LY294002, which induces dephosphorylation of Akt, inhibited cell proliferation. As shown in our previous studies, apoptosis occurred in virus-infected cells within 18 h postinfection. Cellular mRNA transcription, which was reported to be up-regulated in SARS-CoV-infected Caco-2 cells, was not up-regulated in virus-infected Vero E6 cells, partially as a result of apoptosis. These results suggested that inhibition of cell proliferation is regulated by both the phosphatidylinositol 3′-kinase/Akt signaling pathway and by apoptosis in SARS-CoV-infected Vero E6 cells. This is the first study to analyze SARS-CoV-induced cell growth inhibition.

Introduction

Severe acute respiratory syndrome (SARS) is a newly discovered infectious disease caused by a novel coronavirus, SARS coronavirus (SARS-CoV) (Marra, 2003; Rota, 2003). SARS spread from Guangdong province in China to more than 30 countries in late 2002, causing severe outbreaks of atypical pneumonia. Because both the virulence and the mortality rate of this virus are very high, it is important to understand the mechanisms of pathogenesis of SARS-CoV infection for the prevention of SARS.

Our recent studies indicated that signaling pathways are activated upon infection of confluent cultures of Vero E6 cells with SARS-CoV (Mizutani *et al.*, 2004a,b,c). Mitogen-activated protein kinases (MAPKs), including p38, c-Jun N-terminal protein kinase (JNK) and extracellular signal-related kinase (ERK) 1/2, and their MAPKKs, are activated in SARS-CoV-infected Vero E6 cells (Mizutani *et al.*, 2004b). In particular, p38 is involved in induction of apoptosis because a p38 inhibitor was shown to partially prevent apoptosis induced by SARS-CoV infection. Signal transducer and activator of transcription (STAT)-3, which is ordinarily phosphorylated at a tyrosine residue in Vero E6 cells, is dephosphorylated by SARS-CoV-induced activation of p38 (Mizutani *et al.*, 2004a). Akt, which has important antiapoptotic roles, is first phosphorylated at a single serine residue shortly after SARS-CoV infection, and subsequently dephosphorylated during the course of viral infection (Mizutani *et al.*, 2004c). However, threonine phosphorylation of Akt is not detected, and glycogen synthase kinase (GSK)-3β, which is a downstream target of Akt, is slightly phosphorylated in virus-infected cells, suggesting that Akt is unable to prevent virus-induced apoptosis. Interestingly, both Akt and JNK signaling pathways are important for establishing persistent SARS-CoV infection of Vero E6 cells (Mizutani *et al.*, 2005). The weak activation of Akt in cloned Vero E6 cells cannot allow escape from SARS-CoV-induced apoptosis. Thus, the signaling pathway of apoptosis is stronger than

the antiapoptotic pathway in virus-infected Vero E6 cells. Recent studies showed that expression of nucleocapsid, X1, and spike proteins of SARS-CoV can induce apoptosis in cells (He *et al.*, 2003; Surjit *et al.*, 2004; Chang *et al.*, 2004; Tan *et al.*, 2004). Interestingly, nucleocapsid protein induced apoptosis into COS-1 cells in the absence of growth factors, and both JNK and p38 MAPK were up-regulated in nucleocapsid expressing cells, whereas ERK1/2 and Akt were down-regulated (Surjit *et al.*, 2004).

Akt activated by phosphatidylinositol 3′-kinase (PI3K) regulates cell proliferation, the cell cycle and cell survival. A number of proteins, such as Bad, caspase-9 and GSK-3β, have been identified as downstream targets of Akt (Cardone *et al.*, 1998; Pap & Cooper, 1998; Vanhaesebroeck & Alessi, 2000). These proteins are inactivated when phosphorylated by Akt. Activation of Akt by infection with a number of viruses has been reported previously. LMP-1 protein of Epstein–Barr virus has been shown to bind to the p85 subunit of PI3K, resulting in activation of both PI3K and Akt (Dawson *et al.*, 2003). The middle T antigen of murine polyomavirus and the X protein of hepatitis B virus also bind to the p85 subunit of PI3K, leading to activation of Akt (Whitman *et al.*, 1985; Dahl *et al.*, 1998; Lee *et al.*, 2001). Activation of the PI3K/Akt signaling pathway by a variety of viruses is thought to be involved in the establishment of latent and chronic infections by allowing virus-infected cells to escape from apoptosis. Activation of the PI3K/Akt signaling pathway may lead to a delay in apoptosis of host cells, and the virus life cycle might be completed before apoptotic cell death of the host cells. Subsequent apoptosis facilitates the spread of the virus (Roulston *et al.*, 1999). As described above, the PI3K/Akt signaling pathway also promotes cell proliferation. Mirza *et al.* (2004) reported that the PI3K/Akt signaling pathway cooperates with the ERK signaling pathway to promote cell cycle progression in both normal and cancer cells. GSK-3β is a ubiquitously expressed protein-serine/threonine kinase and its activity is inhibited by Akt phosphorylation (Cross *et al.*, 1995). In addition, GSK-3 is now a well-known key component in a large number of cellular processes and disease states, including p53, hypoxia, prions and endoplasmic reticulum stress (Loberg *et al.*, 2002; Song *et al.*, 2002; Watcharasit *et al.*, 2002; Perez *et al.*, 2003). The effects of activation of GSK-3β are mediated through phosphorylation and proteolytic turnover of cyclin D1 (Diehl *et al.*, 1998), resulting in the induction of cell cycle arrest via prevention of retinoblastoma tumor suppressor protein (Rb) hyperphosphorylation.

In the present study, we found that cell proliferation was completely abolished when growing Vero E6 cells were infected with SARS-CoV. Furthermore, we showed that Akt was dephosphorylated without any increase in its phosphorylation upon SARS-CoV infection in subconfluent cultures of Vero E6 cells, in contrast to the tentative up-regulation of phosphorylation of Akt prior to dephosphorylation in confluent cultures of these cells. In our previous study, we showed that caspase-3, which is one of the key factors in apoptosis, was activated within 18 h postinfection (p.i.) in virus-infected cells. Thus, both acute dephosphorylation of Akt and apoptotic events are likely to contribute to the inhibition of cell proliferation of SARS-CoV infected Vero E6 cells.

Materials and methods

Cells and virus

Vero E6 cells were subcultured routinely in 75-cm^3 flasks in Dulbecco's modified Eagle's medium (DMEM) (Sigma, St Louis, MO) supplemented with 0.2 mM L-glutamine, 100 units mL^{-1} penicillin, 100 μg mL^{-1} streptomycin, and 5% (volume in volume, v/v) fetal bovine serum (FBS), and maintained at 37 °C in an atmosphere of 5% CO_2. For use in the experiments, the cells were split once on to 6-, 24- and 96-well tissue culture plate inserts and cultured until they reached 30% or 100% confluence (referred to as subconfluent and confluent, respectively). In the case of subconfluent cell culture, DMEM containing 5% FBS was used. The PI3K inhibitor, LY294002 (Cell Signaling Technology Inc., Beverly, MA), was dissolved in dimethyl sulfoxide (DMSO) at a concentration of 10 mM. DMSO alone was used as a control. SARS-CoV, which was isolated as Frankfurt 1 and kindly provided by Dr. J. Ziebuhr, was used in the present study. Infection was usually performed at a multiplicity of infection of 10.

Western blotting

After virus infection, whole-cell extracts were electrophoresed on either 10% or 10–20% gradient polyacrylamide gels, and transferred electrophoretically onto polyvinylidene fluoride (PVDF) membranes (Immobilon-P, Millipore, Bedford, MA). In the present study, we applied two sets of samples to polyacrylamide gels, and the membranes were either divided into two halves after blotting using a Proto-Blot II AP system (Promega Co., Madison, WI), or they were examined once using a LumiGLO Elite chemiluminescent system (Kirkegaard and Perry Laboratories, Gaithersburg, ML) and then stripped using Restore western blot stripping buffer (Pierce, Rockford, IL) for second detection. The following antibodies, obtained from Cell Signaling Technology Inc., were used in the present study at a dilution of 1 : 1000: rabbit antiphospho Akt (Ser473), rabbit antiphospho Akt (Thr308), rabbit anti-Akt, rabbit antiphospho GSK-3αβ rabbit antiphospho GSK-3β, rabbit anti-GSK-3β, rabbit antiphospho STAT3 (Tyr-705) antibody, rabbit antiphospho STAT3 (Ser-727) antibody, rabbit anti-p38 MAPK (Thr180/Tyr182) antibody, rabbit anti-p38 MAPK antibody,

rabbit antiphospho p44/42 MAPK (Thr202/Tyr204) (=ERK1/2) antibody, rabbit anti-p44/42 MAPK (=ERK1/2) antibody, rabbit antiphospho SAPK/JNK (Thr183/Tyr185) antibody, rabbit antiphospho Rb (Ser795), rabbit antiphospho Rb (Ser807/811) and mouse anti-Rb monoclonal antibody. Mouse anti-STAT3 antibody (diluted 1:2500) was obtained from BD Biosciences (Franklin Lakes, NJ). Mouse anti-β-Actin antibody was purchased from Sigma and used at a dilution of 1:5000. Rabbit anti-SARS nucleocapsid and membrane antibodies were described previously (Mizutani *et al.*, 2004b).

In vitro GSK-3 activation assay

Vero E6 cells were treated with or without epidermal growth factor (EGF) and LY294002 for 10 min, and then cell extracts were obtained using the lysis buffer supplied in the Akt kinase assay kit (Cell Signaling Technology Inc.). Selective immunoprecipitation of Akt was performed using immobilized Akt antibody. After incubation of immunoprecipitated Akt in kinase buffer containing GSK-3β fusion protein and ATP, GSK-3β phosphorylation was analyzed by western blotting using antiphospho GSK-3αβ antibody.

siRNA against GSK-3β

Both GSK-3β small interfering RNA (siRNA) and control siRNA were purchased from Santa Cruz Biotechnology (Santa Cruz, CA). Each siRNA (final concentration 100 nM) was transfected into 30% confluent Vero E6 cells in 96-well plates using the Magnetofection system (OZ Biosciences, Marseille, France) combined with FuGene 6 transfection reagents (Roche, Indianapolis, IL). Efficiency of transfection was determined using fluorescein-labeled Luciferase GL2 duplex (Dharmacon, Lafayette, CO), and we usually obtained nearly 100% transfection efficiency.

RT-PCR

Vero E6 cells were inoculated with SARS-CoV at a multiplicity of infection of 10. Total RNA was extracted from SARS-CoV-infected cells at 24 h p.i. and from mock-infected cells with Isogen (Nippon Gene, Tokyo, Japan). RNAs were reverse-transcribed using SuperScript III (Invitrogen, Carlsbad, CA) and random primers. Semiquantitative PCR amplification was performed using High Fidelity Platinum Taq DNA polymerase (Invitrogen) for 15 to 35 cycles. PCR primers were determined based on sequences with the accession numbers given in the report by Cinatl *et al.* (2004). Primers used in this study were for eukaryotic translation initiation factor 3, subunit 6 (forward 5′-TAATGCAATTCAGACAATGTGTCC-3′, reverse 5′-CTTCT GGAGTCATGTTCAATTTATCTGCC-3′), glyceraldehyde-3-phosphate dehydrogenase (GAPDH) (forward 5′-TGATG ACATCAAGAAGGTGG-3′, reverse 5′-AGCTAGCTAATAG GACTCACTATAGGGTTACTCTCCTTGGAGGCCATGT-3′ including promoter sequence of T7 RNA polymerase), Ets variant gene 5 (forward 5′-CATGGCTACTCTTGGGAACC ACCCGGCC-3′, reverse 5′-ATGTACAACTCAGGTGCAAA TGTTCC-3′), zinc finger protein 384 (forward 5′-CTCTCT CCTTCTCTGCCTACAAAGACCC-3′, reverse 5′-GAAATG GTTACAACAAAGATGGCC-3′), core promoter element-binding protein (forward 5′-GCCGGGAGCCACGGGATTG GGCC-3′, reverse 5′-CGTTTACCTGTTGCCAGTACTCCT CC-3′), Von Hippel–Lindau syndrome (forward 5′-GAC GGCTGGCATGGTGGCTCCC-3′, reverse 5′-ACTCATGGC TCACTGCAGCCTCC-3′), transcription factor 8 (forward 5′-AACCTGTATGCTGTGATTCC-3′, reverse 5′-TCCCAAT TGTACAGCTTAAGAATAAACC-3′), trinucleotide repeat-containing 4 (forward 5′-TCAGCCACAGAGACCCTCCT CC-3′, reverse 5′-AGAAATTAAGAGAGAGAAAAAAATCC-3′), trichorhinophalangeal syndrome 1 (forward 5′-GCTTC AGTTTCATTGTTAACGGGCC-3′, reverse 5′-AAATATTG TTGTTTGGGGGAATCTCC-3′), inhibition of DNA-binding 4 (forward 5′-TATAGATAAATGAGTGACATTTCAT ACC-3′, reverse 5′-TTAAGGATCCAAGCATTTCCTCATCC C-3′), c-fos (forward 5′-CAGAGAGGAGAAACACATCTTC CC-3′, reverse 5′-GATACAATTTGAAAATATCCAGCACC-3′), Friend leukemia virus integration 1 (forward 5′-GACC-GAGTCGTCCATGTACAAGTACCC-3′, reverse 5′-AAAAC GTACAGCTTCTTTCTCAGAACC-3′), early growth response 1 (forward 5′-TGCAATTGTGAGGGACATGCTCA CC-3′, reverse 5′-AGCGCATTCAATGTGTTTATAAGCC-3′) and synoviral sarcoma, X breakpoint 4 (forward 5′-CT GTATTTTCTTGCAGTGTGCC-3′, reverse 5′-AACAGAGT GAGGGGGGCTTGACC-3′). The PCR products were confirmed to be of the correct sizes.

Results

Regulation of cell proliferation upon SARS-CoV infection

Mouse hepatitis virus (MHV), a prototype coronavirus, has been shown to arrest the cell cycle at G0/G1 phase (Chen *et al.*, 2004b). Therefore, we investigated whether SARS-CoV infection suppresses cell proliferation. Subconfluent Vero E6 culture cells were infected with SARS-CoV and the cell number was counted at 24 h p.i. As shown in Fig. 1(a,b), the number of virus-infected cells was not increased at 24 h p.i., whereas that of mock-infected cells was increased by 1.8-fold.

Dephosphorylation of a serine residue of Akt by SARS-CoV infection

As shown in our recent study (Mizutani *et al.*, 2004), a serine residue of Akt was phosphorylated from 8 to 18 h p.i. in

confluent Vero E6 cell cultures, and then dephosphorylated at 24 h p.i.; we concluded that Akt phosphorylation in SARS-CoV-infected cells had low activity (Mizutani *et al.*, 2004). Thus, phosphorylation followed by dephosphorylation of Akt occurred during the course of virus infection. However, it was still unclear whether virus infection was actually responsible for phosphorylation and/or dephosphorylation of Akt.

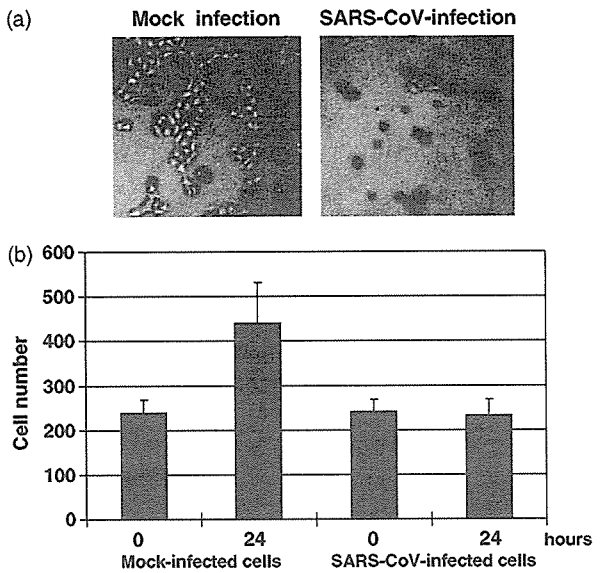

Fig. 1. Prevention of cell proliferation by severe acute respiratory syndrome coronavirus (SARS-CoV) infection. Subconfluent Vero E6 cells were infected with SARS-CoV at a multiplicity of infection of 10. Cell numbers of mock- and virus-infected cells were counted at 24 h postinfection.

To investigate the phosphorylation level of Akt in growing Vero E6 cells, subconfluent cell cultures were used in the present study. As shown in Fig. 2b (mock infection lane), a serine residue of Akt was highly phosphorylated in subconfluent cultures. To examine whether the phosphorylated Akt was up- or down-regulated in subconfluent cell cultures upon SARS-CoV infection, a virus-infection time-course experiment was performed. Cells in subconfluent cultures were infected with the virus at a multiplicity of infection of 10 and western blot analyses were performed using antibodies to viral and cellular proteins at 7, 16 and 23 h p.i. Protein from mock-infected cells was obtained at 7 h. The time-dependent changes of (phospho-)protein level, such as viral nucleocapsid and membrane proteins, the kinetics of MAPKs, including p38, JNK and ERK 1/2, and STAT-3 in virus-infected subconfluent Vero E6 cells were similar to those in confluent cells after viral infection (Fig. 2a,b; Mizutani *et al.*, 2004b). As shown in Fig. 2a, only the kinetics of Ser473-phosphorylation of Akt were different. Akt, which was always phosphorylated in subconfluent cells, was dephosphorylated at 16 and 23 h p.i. On the other hand, Akt in mock-infected cells was continuously phosphorylated from 7 to 24 h p.i. (data not shown; Fig. 2c). We measured the

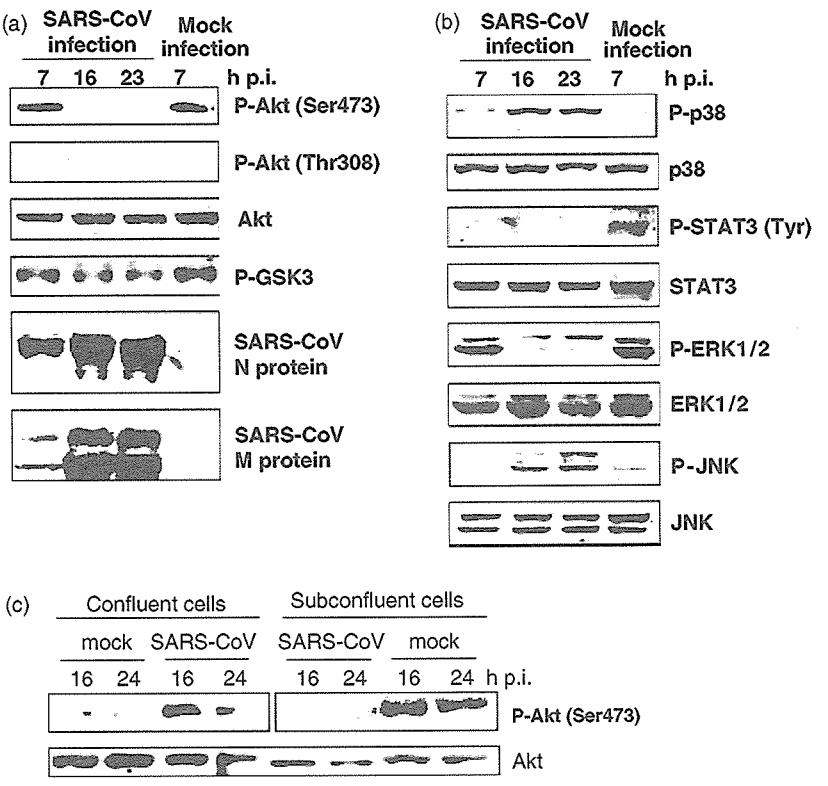

Fig. 2. Acute dephosphorylation of Akt serine by severe acute respiratory syndrome coronavirus (SARS-CoV) infection. (a,b) Subconfluent Vero E6 cells were infected with SARS-CoV at a multiplicity of infection of 10 and then western blot analysis was performed using anti-Akt, glycogen synthase kinase (GSK)-3β, viral proteins, p38, signal transducer and activator of transcription (STAT)3, extracellular signal-related kinase (ERK)1/2 and c-Jun nucleocapsid-terminal protein kinase (JNK) antibodies. (c) Confluent and subconfluent cells were infected with SARS-CoV at a multiplicity of infection of 10 and western blot analysis was performed. Proteins equivalent to same cell number were applied to the gel. p.i., postinfection.

densities of Ser473-phosphorylated Akt of mock-infected subconfluent cells and SARS-CoV-infected confluent cells at 16 h p.i. (Fig. 2c) using the LAS-3000 mini system (Fuji Photo Film Co. Ltd., Tokyo, Japan). The amount of phosphorylated Akt of mock-infected subconfluent cells was 4.8-fold higher than that of SARS-CoV-infected confluent cells. GSK-3β was also dephosphorylated in SARS-CoV-infected subconfluent cells. We next investigated whether Akt was phosphorylated in virus-infected subconfluent cell cultures before 7 h p.i. The phosphorylation level of Akt-serine was not up-regulated at 2, 4 or 6 h p.i. (data not shown). The phosphorylation of GSK-3 were also similar at 2 and 6 h p.i. (data not shown). In addition, phosphorylation level of Akt kinase did not significantly change from 7 to 23 h p.i. (data not shown). These results suggested that SARS-CoV infection induces dephosphorylation of a serine residue of Akt in subconfluent cultures, without tentative up-regulation of phosphorylation prior to dephosphorylation.

Activity of Akt in subconfluent cells

To investigate whether Akt serine phosphorylation represented a biologically active kinase in subconfluent cells, we examined the *in vitro* kinase activity of phosphorylated Akt. Subconfluent Vero E6 cells treated with EGF for 10 min or LY294002 for 1 h were lysed and Ser473-phosphorylated Akt in the cell lysate was precipitated with anti-Akt antibody. GSK-3β protein was added to the immunoprecipitated Akt with ATP, and western blotting was performed using antiphosphorylated GSK-3α/β antibody. As shown in Fig. 3, the level of phosphorylation of GSK-3 in EGF-treated cells was higher than that in nontreated cells. On the other hand, phosphorylation of GSK was not detected in cells treated with the PI3K inhibitor, LY294002. These results strongly suggested that Akt in subconfluent Vero E6 cell cultures was phosphorylated mainly at serine residues and had kinase activity.

Regulation of cell proliferation by Akt

The level of phosphorylated GSK-3β was decreased in virus-infected cells, possibly as a result of down-regulation of Akt

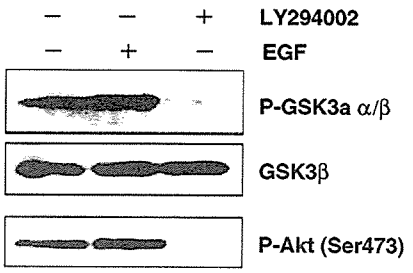

Fig. 3. Phosphorylation status of Akt in subconfluent cells. Epidermal growth factor and LY294002 were added to subconfluent Vero E6 cells for 10 min and 1 h, respectively. The cell lysates were precipitated using anti-Akt antibody. Glycogen synthase kinase (GSK)-3β protein was added to the immunoprecipitated Akt with ATP, and western blot analysis was performed using antiphosphorylated GSK-3α/β and antiphosphorylated Akt (Ser) antibodies.

activation (Fig. 2a). Because one of the important roles of Akt is in cell cycle regulation by preventing GSK-3β-mediated phosphorylation and degradation of cyclin D1 (Diehl *et al.*, 1998), we examined whether GSK-3β regulates the proliferation of Vero E6 cells. Vero E6 cells were transfected with GSK-3β siRNA, and western blot analysis was performed 48 h later to detect the total amount of GSK-3β protein. As shown in Fig. 4a, the total amount of GSK-3β was reduced markedly by the siRNA, and the level of phosphorylated GSK-3β was reduced. However, GSK-3β siRNA-treated cells exhibited similar growth to those treated with control siRNA (Fig. 4b). The total amount of Rb and phosphorylated Rb was not affected by GSK-3β siRNA. The hyperphosphorylation form of Rb is known to be phosphorylated at least at Ser795, Ser807, and Ser811 (Faenza *et al.*, 2000; Jiang, 2002; Shibata & Nakamura, 2002), and hyperphosphorylation of Rb at Ser795 to release E2F is a critical step in the G1–S transition (Harbour & Dean, 2000).

We next investigated whether inhibition of the PI3K/Akt signaling pathway inhibits cell proliferation of Vero E6 cells. As shown in Fig. 5, complete inhibition by the PI3K inhibitor, LY294002, was observed at 48 h. We confirmed that serine residues of Akt were dephosphorylated in LY294002-treated cells in our previous study. These results

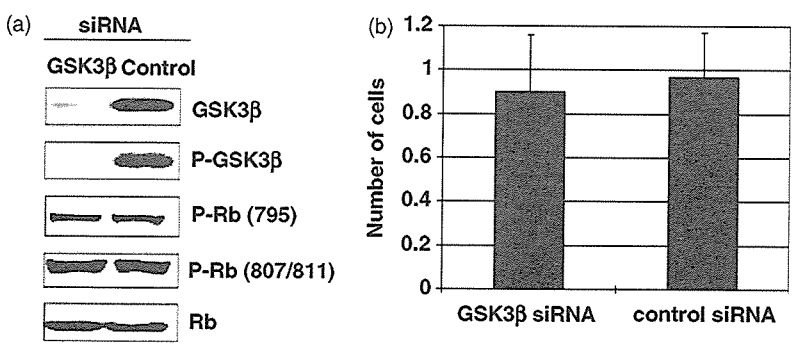

Fig. 4. Relationship between glycogen synthase kinase (GSK)-3β and Rb in cell proliferation. (a) GSK-3β small interfering RNA (siRNA) was transfected into subconfluent Vero E6 cells for 48 h and then western blot analysis was performed. (b) Cell number was determined using a WST-1 cell counting kit (Dojin, Kumamoto, Japan).

suggested that activation of Akt in subconfluent Vero E6 cells plays important roles in cell proliferation, and that down-regulation of Akt activity in SARS-CoV-infected cells prevents cell proliferation.

Down-regulation of cellular mRNAs in virus-infected cells

Although LY294002 inhibits proliferation of Vero E6 cells, apoptotic cell death was not induced by treatment with this agent (10 μM) for 48 h by western blot analysis using anti-cleaved caspase-3 (data not shown). As indicated in our previous study, apoptotic events progress in virus-infected cells. Therefore, these findings strongly suggested that both events Akt-dephosphorylation and apoptosis are responsible for the inhibition of cell proliferation in SARS-CoV-infected cells. We feel that transcriptional activity in virus-infected cells is important for understanding the viability of cells. Cinatl *et al.* (2004) demonstrated that SARS-CoV infection regulates cellular gene expression in a SARS-CoV-permissive cell line, Caco-2, at 24 h p.i. using high-density oligonucleotide arrays. We focused on up-regulated genes related to transfection factors, because several signaling pathways, which generally play important roles in the activation of transcription factors, are activated in SARS-CoV-infected Vero E6 cells. We selected 14 genes (including the housekeeping gene, GAPDH) that were shown previously to be up-regulated by several stimuli (Cinatl *et al.*, 2004), and semi-quantitative reverse transcription PCR (RT-PCR) was performed using total RNA extracted from virus-infected confluent Vero E6 cells at 24 h p.i. The amount of total RNA was adjusted by the level of ribosomal RNA (Fig. 6s). Figure 6(b,c) shows genes that were down-regulated and that showed similar expression upon SARS-CoV-infection compared to mock-infected cells, respectively. Eukaryotic translation initiation factor 3, Ets variant gene 5, Zinc finger protein

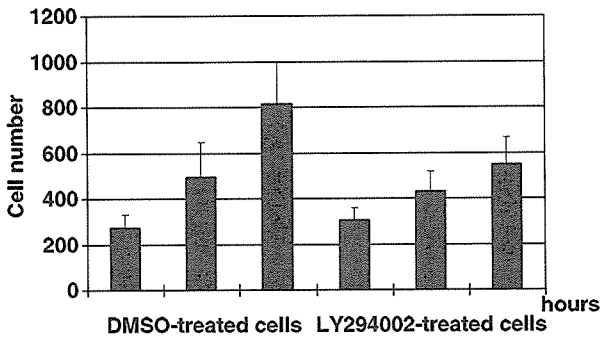

Fig. 5. Prevention of cell proliferation by LY294002 treatment. Subconfluent Vero E6 cells were treated with LY294002 at a concentration of 10 μM. Cell numbers of mock- and LY294002-treated cells were counted at 24 and 48 h postinfection.

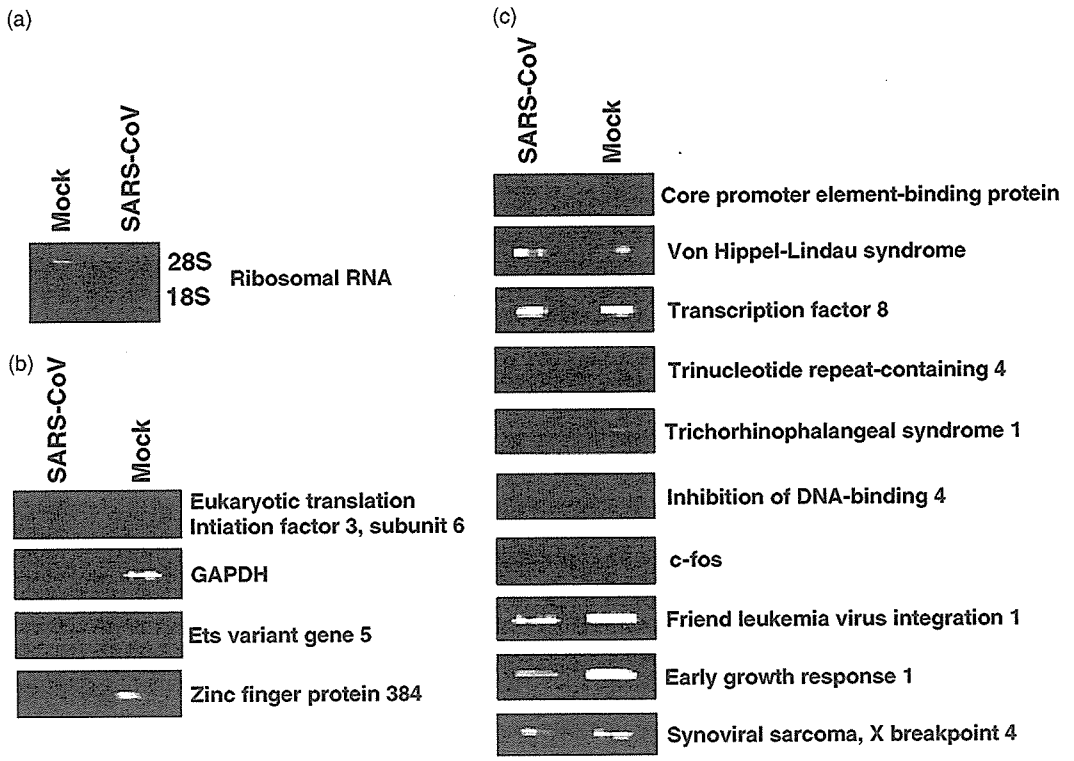

Fig. 6. Semiquantitative reverse transcription PCR (RT-PCR) of cellular transcripts. Total RNAs were extracted from virus-infected and mock-infected confluent Vero E6 cells at 24 h postinfection. Transcripts of cellular genes were assessed for their relative abundance by RT-PCR.

384 and GAPDH were down-regulated in SARS-CoV-infected cells. These results suggested that transcriptional shut-off occurred in particular (or in many) cellular mRNAs due to SARS-CoV infection, and that virus-infected cells are not proliferative due to Akt dephosphorylation and apoptosis.

Discussion

In the present study, we focused on the different kinetics of the phosphorylation status of Akt in subconfluent Vero E6 cells upon SARS-CoV infection. Akt-phosphorylation is up- and down-regulated by virus infection in the confluent cells, as shown in our previous report (Mizutani *et al.*, 2004), but is down-regulated by virus infection in subconfluent cells. Therefore, one of the aims of the present study was to determine whether SARS-CoV has the potential for up- or down-regulation of Akt-phosphorylation in Vero E6 cells. Akt was phosphorylated in growing mock-infected cells (i.e. 30% confluency), whereas it was dephosphorylated in confluent cell cultures. An Akt-binding protein, carboxyl-terminal modulator protein (CTMP), is a well-known negative regulatory component of the Akt (Maira *et al.*, 2001). CTMP, which binds to Akt, reduces the activity of Akt by inhibiting phosphorylation on serine and threonine residues. We found that the level of CTMP was below the limit of detection at 0–24 h p.i. in subconfluent virus-infected cells (data not shown), suggesting that dephosphorylation of Akt in subconfluent cell cultures upon viral infection was not regulated by CTMP. Although we obtained proteins from SARS-CoV-infected cells at different time points from 5 to 24 h p.i. in at least six experiments and performed western blot analysis using anti-phospho Akt (Ser) antibody, we were not able to find up-regulation of Akt-phosphorylation in SARS-CoV-infected subconfluent Vero E6 cells. Therefore, we concluded in this study that SARS-CoV has a potential of down-regulation of Akt-phosphorylation. It may be possible that SARS-CoV infection induces activation of Akt phosphatase(s).

In our previous study, we showed that apoptotic events, such as caspase-3 activation and DNA ladder formation, were detected in SARS-CoV-infected Vero E6 cells at 18 and 24 h p.i., respectively (Mizutani *et al.*, 2004b,c). We could not find any up-regulated genes in SARS-CoV-infected Vero E6 cells, in contrast with SARS-CoV-infected Caco-2 cells, in which several genes were demonstrated to be up-regulated (Cinatl *et al.*, 2004). This may have resulted from the faster progression of apoptosis and more rapid production of virus particles in infected Vero E6 as compared with Caco-2 cells. Thus, transcriptional shut-off in virus-infected cells may prevent cell proliferation with dephosphorylation of Akt.

In conclusion, the results of the present study suggested that SARS-CoV-infection affected Akt signaling pathways and gene expression. Down-regulation of Akt activity and the processing of apoptotic events in virus-infected cells may prevent cell proliferation. We assume that these phenomena are at least partly involved in the pathogenesis of SARS-CoV infection.

Acknowledgements

We thank Drs Y. Goto (University of Tokyo, Japan), M. Funaba (Azubu University), K. Nakagaki (National Institute of Infectious Diseases, Japan) and S. Makino (University of Texas Medical Branch at Galveston, USA) for helpful suggestions. We also thank Ms M. Ogata (National Institute of Infectious Diseases, Japan) for her assistance. This work was supported in part by a grant-in-aid from the Ministry of Health, Labor, and Welfare of Japan, Japan Society for Promotion of Science, and the Japan Health Science Foundation, Tokyo, Japan.

References

Cardone MH, Roy N, Stennicke HR, Salvesen GS, Franke TF, Stanbridge E, Frisch S & Reed JC (1998) Regulation of cell death protease caspase-9 by phosphorylation. *Science* **282**: 1318–1321.

Chang YJ, Liu CY, Chiang BL, Chao YC & Chen CC (2004) Induction of IL-8 release in lung cells *via* activator protein-1 by recombinant baculovirus displaying severe acute respiratory syndrome-coronavirus spike proteins: identification of two functional regions. *J Immunol* **173**: 7602–7614.

Chen CJ, Sugiyama K, Kubo H, Huang C & Makino S (2004) Murine coronavirus nonstructural protein p28 arrests cell cycle in G0/G1 phase. *J Virol* **78**: 10410–10419.

Cinatl J Jr, Hoever G, Morgenstern B, Preiser W, Vogel JU, Hofmann WK, Bauer G, Michaelis M, Rabenau HF & Doerr HW (2004) Infection of cultured intestinal epithelial cells with severe acute respiratory syndrome coronavirus. *Cell Mol Life Sci* **61**: 2100–2112.

Cross DAE, Alessi DR, Cohen P, Andjelkovich M & Hemmings BA (1995) Inhibition of glycogen synthase kinase-3 by insulin mediated by protein kinase B. *Nature* **378**: 785–789.

Dahl J, Jurczak A, Cheng LA, Baker DC & Benjamin TL (1998) Evidence of a role for phosphatidylinositol 3-kinase activation in the blocking of apoptosis by polyomavirus middle T antigen. *J Virol* **72**: 3221–3226.

Dawson CW, Tramountanis G, Eliopoulos AG & Young LS (2003) Epstein–Barr virus latent membrane protein 1 (LMP1) activates the phosphatidylinositol 3-kinase/Akt pathway to promote cell survival and induce actin filament remodeling. *J Biol Chem* **278**: 3694–3704.

Diehl JA, Cheng M, Roussel MF & Sherr CJ (1998) Glycogen synthase kinase-3beta regulates cyclin D1 proteolysis and subcellular localization. *Genes Dev* **12**: 3499–3511.

Faenza I, Matteucci A, Manzoli L, Billi AM, Aluigi M, Peruzzi D, Vitale M, Castorina S, Suh PG & Cocco L (2000) A role for

nuclear phospholipase Cbeta 1 in cell cycle control. *J Biol Chem* **275**: 30520–30524.

Harbour JW & Dean DC (2000) Rb function in cell-cycle regulation and apoptosis. *Nat Cell Biol* **2**: 65–67.

He R, Leeson A, Andonov A, *et al.* (2003) Activation of AP-1 signal transduction pathway by SARS coronavirus nucleocapsid protein. *Biochem Biophys Res Commun* **311**: 870–876.

Jiang JD, Denner L, Ling YH, *et al.* (2002) Double blockade of cell cycle at G1-S transition and M phase by 3-iodoacetamido benzoyl ethyl ester, a new type of tubulin ligand. *Cancer Research* **62**: 6080–6088.

Lee YI, Kang-Park S & Do SI (2001) The hepatitis B virus-X protein activates a phosphatidylinositol 3-kinase-dependent survival signaling cascade. *J Biol Chem* **276**: 16969–16977.

Loberg RD, Vesely E & Brosins FC III (2002) Enhanced glycogen synthase kinase-3beta activity mediates hypoxia-induced apoptosis of vascular smooth muscle cells and is prevented by glucose transport and metabolism. *J Biol Chem* **277**: 41667–41673.

Maira SM, Galetic I, Brazil DP, Kaech S, Ingley E, Thelen M & Hemmings BA (2001) Carboxyl-terminal modulator protein (CTMP), a negative regulator of PKB/Akt and v-Akt at the plasma membrane. *Science* **294**: 374–380.

Marra MA, Jones SJ, Astell CR, *et al.* (2003) The Genome sequence of the SARS-associated coronavirus. *Science* **300**: 1399–1404.

Mirza AM, Gysin S, Malek N, Nakayama K, Roberts JM & McMahonn M (2004) Cooperative regulation of the cell division cycle by the protein kinases RAF and AKT. *Mol Cell Biol* **24**: 10868–10881.

Mizutani T, Fukushi S, Murakami M, Hirano T, Saijo M, Kurane I & Morikawa S (2004a) Tyrosine dephosphorylation of STAT3 in SARS coronavirus-infected Vero E6 cells. *FEBS Lett* **577**: 187–192.

Mizutani T, Fukushi S, Saijo M, Kurane I & Morikawa S (2004b) Phosphorylation of p38 MAPK and its downstream targets in SARS coronavirus-infected cells. *Biochem Biophys Res Commun* **319**: 1228–1234.

Mizutani T, Fukushi S, Saijo M, Kurane I & Morikawa S (2004c) Importance of Akt signaling pathway for apoptosis in SARS-CoV-infected Vero E6 cells. *Virology* **327**: 169–174.

Mizutani T, Fukushi S, Saijo M, Kurane I & Morikawa S (2005) JNK and PI3K/Akt signaling pathways are required for establishing persistent SARS-CoV-infection in Vero E6 cells. *Biochim Biophys Acta* **1741**: 4–10.

Pap M & Cooper GM (1998) Role of glycogen synthase kinase-3 in the phosphatidylinositol 3-Kinase/Akt cell survival pathway. *J Biol Chem* **273**: 19929–19932.

Perez M, Rojo AI, Wandosell F, Diaz-Nido J & Avila J (2003) Prion peptide induces neuronal cell death through a pathway involving glycogen synthase kinase 3. *Biochem J* **372**: 129–136.

Rota PA, *et al.* (2003) Characterization of a novel coronavirus associated with severe acute respiratory syndrome. *Science* **300**: 1394–1399.

Roulston A, Marcellus RC & Branton PE (1999) Viruses and apoptosis. *Annu Rev Microbiol* **53**: 577–628.

Shibata Y & Nakamura T (2002) Defective flap endonuclease 1 activity in mammalian cells is associated with impaired DNA repair and prolonged S phase delay. *J Biol Chem* **277**: 746–754.

Song L, De Sarno P & Jope RS (2002) Central role of glycogen synthase kinase-3beta in endoplasmic reticulum stress-induced caspase-3 activation. *J Biol Chem* **277**: 44701–44708.

Surjit M, Liu B, Jameel S, Chow VT & Lal SK (2004) The SARS coronavirus nucleocapsid protein induces actin reorganization and apoptosis in COS-1 cells in the absence of growth factors. *Biochem J* **383**: 13–18.

Tan YJ, Fielding BC, Goh PY, Shen S, Tan TH, Lim SG & Hong W (2004) Overexpression of 7a, a protein specifically encoded by the severe acute respiratory syndrome coronavirus, induces apoptosis *via* a caspase-dependent pathway. *J Virol* **78**: 14043–14047.

Vanhaesebroeck B & Alessi DR (2000) The PI3K-PDK1 connection: more than just a road to PKB. *Biochem J* **346**: 561–576.

Watcharasit P, Bijur GN, Zmijewski JW, Song L, Zmijewska A, Chen X, Johnson GV & Jope RS (2002) Direct, activating interaction between glycogen synthase kinase-3beta and p53 after DNA damage. *Proc Natl Acad Sci USA* **99**: 7951–7955.

Whitman M, Kaplan DR, Schaffhausen B, Cantley L & Roberts TM (1985) Association of phosphatidylinositol kinase activity with polyoma middle-T competent for transformation. *Nature* **315**: 239–242.

FEBS Letters 580 (2006) 1417–1424

Regulation of p90RSK phosphorylation by SARS-CoV infection in Vero E6 cells

Tetsuya Mizutani*, Shuetsu Fukushi, Masayuki Saijo, Ichiro Kurane, Shigeru Morikawa

Special Pathogens Laboratory, Department of Virology 1, National Institute of Infectious Diseases, Gakuen 4-7-1, Musashimurayama, Tokyo 208-0011, Japan
Department of Bacteriology 2, National Institute of Infectious Diseases, Gakuen 4-7-1, Musashimurayama, Tokyo 208-0011, Japan

Received 1 December 2005; revised 10 January 2006; accepted 17 January 2006

Available online 30 January 2006

Edited by Hans-Dieter Klenk

Abstract **The 90 kDa ribosomal S6 kinases (p90RSKs) are a family of broadly expressed serine/threonine kinases with two kinase domains activated by extracellular signal-regulated protein kinase in response to many growth factors. Our recent study demonstrated that severe acute respiratory syndrome (SARS)-coronavirus (CoV) infection of monkey kidney Vero E6 cells induces phosphorylation and dephosphorylation of signaling pathways, resulting in apoptosis. In the present study, we investigated the phosphorylation status of p90RSK, which is a well-known substrate of these signaling pathways, in SARS-CoV-infected cells. Vero E6 mainly expressed p90RSK1 and showed weak expression of p90RSK2. In the absence of viral infection, Ser221 in the N-terminal kinase domain was phosphorylated constitutively, whereas both Thr573 in the C-terminal kinase domain and Ser380 between the two kinase domains were not phosphorylated in confluent cells. Ser380, which has been reported to be involved in autophosphorylation by activation of the C-terminal kinase domain, was phosphorylated in confluent SARS-CoV-infected cells, and this phosphorylation was inhibited by SB203580, which is an inhibitor of p38 mitogen-activated protein kinases (MAPK). Phosphorylation of Thr573 was not upregulated in SARS-CoV-infected cells. Thus, in virus-infected cells, phosphorylation of Thr573 was not necessary to induce phosphorylation of Ser380. On the other hand, Both Thr573 and Ser380 were phosphorylated by treatment with epidermal growth factor (EGF) in the absence of p38 MAPK activation. Ser220 was constitutively phosphorylated despite infection. These results indicated that phosphorylation status of p90RSK by SARS-CoV infection is different from that by stimulation of EGF. This is the first detailed report regarding regulation of p90RSK phosphorylation by virus infection.**

Keywords: 90 kDa ribosomal S6 kinases; Phosphorylation; Severe acute respiratory syndrome

1. Introduction

The signaling pathway of extracellular signal-regulated kinase (ERK) regulates cellular processes, including growth, cell proliferation, survival, and motility [1]. The p90 ribosomal S6 kinases (RSK), a family of serine/threonine kinases, are important substrates of ERK [2]. The RSK family consists of four isoforms (RSK1, 2, 3, and 4) and two structurally related RSK-like protein kinases (RLPK/MSK1) and RSK-B (MSK2) in humans [2–5]. Members of the RSK family contain two distinct kinase domains. The C-terminal kinase domain is thought to be involved in autophosphorylation at the critical step in 90 kDa ribosomal S6 kinase (p90RSK) activation [6–8]. On the other hand, the N-terminal kinase domain is capable of phosphorylation of substrates. Recent studies have clarified the mechanisms of activation of p90RSK. p90RSK1 is phosphorylated at Thr573 in the activation loop of the C-terminal kinase domain by ERK because the C-terminal of p90RSK has an ERK docking site [9,10]. Autophosphorylation at Ser380 in the linker region is thought to be induced by activation of the C-terminal kinase domain [11], and then PDK1 phosphorylates at Ser221 in the activation loop of the N-terminal kinase domain [12–14].

p90RSK is thought to have multiple functions. In quiescent cells, p90RSK is present in the cytoplasm, and p90RSK activated via the ERK signaling pathway by growth factors is imported into the nucleus. p90RSK activates nuclear factor-κB by phosphorylation of Iκ-B and phosphorylates the transcription factors, c-Fos and cAMP-response element-binding protein (CREB) [2]. It has been shown that p90RSK plays important roles in apoptosis and the cell cycle. p90RSK phosphorylates Bad [15,16] and C/EBPβ [17], which protects cells against apoptosis. Furthermore, p90RSK phosphorylates and inhibits Myt1, which is a p34cdc2 inhibitory kinase, resulting in G2 arrest in *Xenopus* extracts [18,19]. In mouse oocytes, Emi1 and p90RSK2 cooperate to induce metaphase arrest [20]. p90RSK also functions as a serum-stimulated Na^+/H^+ exchanger-1 kinase and regulates its activity [21]. Recently, it has been shown that p90RSK activation induces H_2O_2-mediated cardiac troponin I phosphorylation, which depresses the acto-myosin interaction and is important during the progression of heart failure [21]. Thus, p90RSK has been demonstrated to play key roles in regulating cellular functions in the ERK signaling pathway in vitro and in vivo.

Severe acute respiratory syndrome (SARS) is a newly discovered infectious disease caused by a novel coronavirus, SARS coronavirus (SARS-CoV) [22,23], which spread to more than 30 countries in late 2002, causing severe outbreaks of atypical pneumonia. Our recent studies using the monkey kidney cell line, Vero E6, demonstrated that a variety of signaling pathways are activated upon infection with SARS-CoV. Especially, p38 mitogen-activated protein kinase (MAPK) is thought to be involved in induction of apoptosis because a p38 inhibitor was

*Corresponding author. Fax: +81 42 564 4881.
E-mail address: tmizutan@nih.go.jp (T. Mizutani).

0014-5793/$32.00
doi:10.1016/j.febslet.2006.01.066

able to partially prevent cytopathic effects induced by SARS-CoV infection [24]. Signal transducer and activator of transcription (STAT)-3, which is ordinarily phosphorylated at a tyrosine residue, is dephosphorylated by SARS-CoV-induced activation of p38 [25]. c-Jun N-terminal protein kinase (JNK) and Akt are important for establishing persistent SARS-CoV infection [26]. In confluent virus-infected cells, Akt is first phosphorylated at a single serine residue shortly after SARS-CoV infection, and subsequently dephosphorylated during the course of viral infection [27], whereas Akt, which is ordinary phosphorylated at a serine residue, was dephosphorylated by SARS-CoV infection without any upregulation of its phosphorylation in subconfluent cells [28]. This downregulation of Akt phosphorylation induces inhibition of cell proliferation by SARS-CoV infection and weak activation of Akt cannot induce escape from SARS-CoV-induced apoptosis. Nucleocapsid protein, X1 and spike proteins of SARS-CoV are able to induce apoptosis in their expressing cells [29–32]. Especially, N protein is able to upregulation of phosphorylation of JNK and p38 MAPK, but not ERK and Akt [29]. Although ERK was shown to be phosphorylated in SARS-CoV-infected cells [25], the function is not clear. p90RSK is a well-known substrate for ERK as described above.

In the present study, we showed that Ser380 of p90RSK, which is thought to be auto-phosphorylated after activation of the C-terminal kinase domain, is phosphorylated without upregulation of Thr573 phosphorylation in the C-terminal kinase domain, in SARS-CoV-infected Vero E6 cells. Furthermore, we demonstrated that activation of p38 MAPK was responsible for phosphorylation of Ser380 in virus-infected cells. These results indicated signaling pathways, which are different from those induced by growth factor, contribute to phosphorylation of p90RSK in SARS-CoV-infected cells.

2. Materials and methods

2.1. Cells and virus

Vero E6 cells were subcultured routinely in 75-cm^3 flasks in Dulbecco's modified Eagle's medium (DMEM; Sigma, St. Louis, MO, USA) supplemented with 0.2 mM L-glutamine, 100 units/ml penicillin, 100 μg/ml streptomycin, and 5% (v/v) fetal bovine serum (FBS), and maintained at 37 °C in an atmosphere of 5% CO_2. For use in the experiments, the cells were split once onto 6- and 24-well tissue culture plate inserts and cultured under subconfluent and confluent conditions. SARS-CoV, which was isolated as Frankfurt 1 and kindly provided by Dr. J. Ziebuhr, was used in the present study. Infection was usually performed at a multiplicity of infection (m.o.i.) of 10. The number of cells was counted using the WST-1 cell proliferation assay system (Takara, Shiga, Japan).

2.2. Inhibitor

The p38 MAPK inhibitor, SB203580, which was purchased from Calbiochem (La Jolla, CA, USA), was dissolved in dimethyl sulfoxide (DMSO) at a concentration of 10 mM. The same volume of DMSO alone was used as a control. As shown in previous reports [24,27], SB203580 and PD98059 had no effect on viral replication including viral protein synthesis.

2.3. Western blotting

The whole-cell extracts were electrophoresed on 5–20% gradient polyacrylamide gels, and transferred electrophoretically onto PVDF membranes (Immobilon-P; Millipore, Bedford, MA, USA). In the present study, we applied two sets of samples to polyacrylamide gels, and the membranes were divided into two halves after blotting using a LumiGLO Elite chemiluminescent system (Kirkegaard and Perry Laboratories, Gaithersburg, ML, USA). When it was necessary to strip the membranes, Restore Western blot stripping buffer (Pierce, Rockford, IL, USA) was used. The following antibodies, obtained from Cell Signaling Technology Inc. (Beverly, MA, USA), were used in the present study at a dilution of 1:1000: rabbit anti-phospho Akt (Ser473) antibody, rabbit anti-Akt antibody, rabbit anti-phospho-PDK1 (Ser241) antibody, rabbit anti-phospho STAT3 (Tyr-705) antibody, rabbit anti-p38 MAPK (Thr180/Tyr182) antibody, rabbit anti-p38 MAPK antibody, rabbit anti-phospho-ERK1/2 (Thr202/Tyr204) antibody, rabbit anti-ERK antibody, rabbit anti-phospho-MEK1/2 (Ser217/221) antibody, rabbit anti-MEK1/2 antibody, rabbit anti-p90RSK1/2/3 antibody, rabbit anti-cleaved Caspase-3 (Asp175) antibody, rabbit anti-cleaved Caspase-7 (Asp198) antibody. Rabbit Mouse anti-STAT3 antibody (diluted 1:2500) was obtained from BD Biosciences (Franklin Lakes, NJ, USA). Rabbit anti-p90RSK1 monoclonal antibody, which was purchased from Epitomics, Inc. (Burlingame, CA, USA), was diluted at 1:1000. Rabbit anti-p90RSK2 (C-term), p90RSK3 (Mid) and p90RSK4 (N-term) were purchased from Zymed Laboratory, Inc. (South San Francisco, CA, USA). Anti-p90RSK2 and 4 antibodies were diluted 1:250, and anti-p90RSK3 was diluted 1:500. Rabbit anti-PARP p85 fragment antibody was purchased from Promega (Madison, WI, USA) and diluted 1:100. Mouse anti-β-actin antibody was purchased from Sigma (St. Louis, MO, USA) and used at a dilution of 1:5000. Rabbit anti-SARS N and M antibodies were described previously [24]. K562 and Jurkat cell lysates were purchased from Clontech Laboratories Inc. (Mountain View, CA, USA).

3. Results

3.1. Signaling pathways in SARS-CoV-sensitive cell lines

As shown in Fig. 1, SARS-CoV-infected confluent Vero E6 cells induced phosphorylation or dephosphorylation of signaling pathways as also described in previous studies [24,27,28]. The cytopathic effects (CPEs) were observed in Vero E6 cells at 24-h post-infection (h.p.i.). DNA fragmentation as an indicator of apoptosis was detected at 24 h.p.i. [24]. Among the signaling pathways activated by SARS-CoV infection, p38 MAPK is thought to act as a pro-apoptotic signaling pathway, whereas Akt has an anti-apoptotic effect. Vero cells, the parental cells of Vero E6, are also sensitive to SARS-CoV infection. However, the time point of the appearance of CPE on Vero cells by SARS-CoV infection is later than that of Vero E6 cells at 24 h.p.i. (data not shown). As shown in Fig. 1A, nucleocapsid (N) protein of SARS-CoV was detected at 17 h.p.i. in both cell lines. The level of N protein in Vero cells was only slightly lower than that in Vero E6 cells, indicating that replication of SARS-CoV is not markedly different between the two cell lines. Anti-apoptotic Akt was phosphorylated at 17 h.p.i. in both cell lines, and was dephosphorylated at 27 h.p.i. (Fig. 1B). Our previous study indicated that phosphorylation level of Akt around 17 h.p.i. is only 20% of phosphorylated Akt in growing cells [28]. Therefore, this low level of activation cannot prevent apoptosis by SARS-CoV infection. Fig. 1B also shows that ERK was phosphorylated at 17 h.p.i. in both cell lines, similar to the observations regarding Akt. The apoptotic markers, PARP (p85) and cleaved caspase-3 and -7, were detected in Vero E6 and Vero cells at 27 and 44 h.p.i., respectively (Fig. 1A). The p38 MAPK in virus-infected Vero E6 and Vero cells was phosphorylated at 17 and 27 h.p.i., respectively (Fig. 1A). Tyrosine of STAT3 was also dephosphorylated via phosphorylation of p38 MAPK as reported previously [25]. Thus, SARS-CoV-induced apoptosis related to time-dependent activation of the pro-apoptotic signaling pathway, p38 MAPK. Taken together, these results suggested that substrates

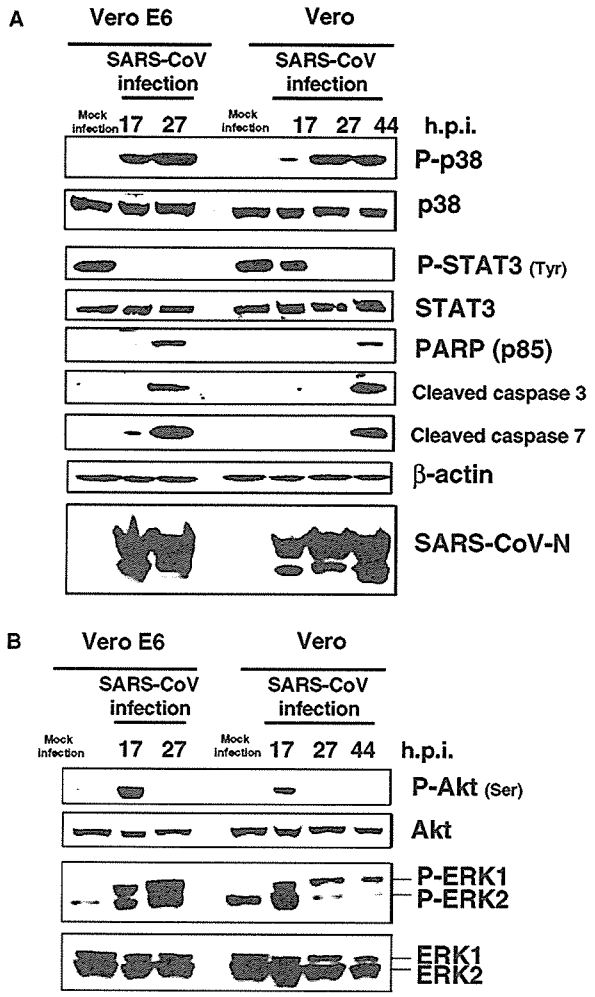

Fig. 1. Phosphorylation of signaling pathways in SARS-CoV-infected cells. Vero and Vero E6 cells were prepared at confluence in 24-well plates and the cells were infected with SARS-CoV at 10 m.o.i. Protein samples were obtained at 17, 24, and 44 h.p.i. The protein of Vero E6 cells at 44 h.p.i. could not be obtained due to strong morphological changes caused by apoptosis. Western blotting analyses were performed to examine signaling pathways (A) and apoptotic marker proteins (B).

of PI3K/Akt, ERK1/2, and p38 MAPK are important for understanding the cytopathic effects of SARS-CoV infection.

3.2. Phosphorylation of p90RSK Ser221 in Vero E6 cells

p90RSK is phosphorylated by both PDK-1 and ERK [2,13,14]. Ser221 of p90RSK1 is phosphorylated by PDK-1 and Thr359, Ser363, and Thr573 of p90RSK-1 are phosphorylated by ERK. p90RSK is thought to play important roles in apoptosis and the cell cycle. Both PI3K/Akt and ERK signaling pathways are activated early post-infection with SARS-CoV in both Vero and Vero E6 cells (Fig. 1B). Therefore, p90RSK may be a target of both signaling pathways in SARS-CoV-infected cells. At least four species of p90RSK (p90RSK1, 2, 3, and 4) has been reported to date [2–5]. We used anti-p90RSK antibodies, which do not cross-react with other p90RSK family members, as described in the legend of Fig. 2. We measured densities of RSK1 and 2 bands in Vero E6 cells using LAS-3000 mini system (Fuji Photo Film Co.

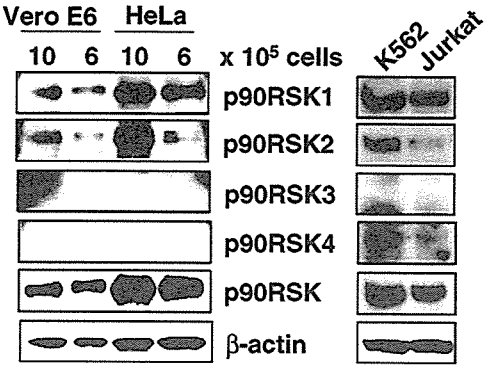

Fig. 2. p90RSK family expressed in Vero E6 cells. Vero E6 cells were prepared at densities of 1×10^6 and 0.6×10^5 in 6-well plates. HeLa cells, a clonal cell line for another study, were used as controls. Both K562 and Jurkat cell lysates were obtained from Clontech Laboratories Inc. Western blotting analysis was performed using the same amounts of protein. According to the antibody product data sheets, anti-human p90RSK1 monoclonal antibody (Epitomics) does not cross-react with other RSK family members. Anti-human and mouse p90RSK2 antibody (Zymed) does not react with overexpressed p90RSK1, 3, or 4. Anti-human p90RSK3 antibody (Zymed) does not react with overexpressed p90RSK1, 2, or 4. Anti-human p90RSK antibody (Zymed) does not react with p90RSK1, 2, or 3. Anti-p90RSK1/2/3 antibody (Cell Signaling) detects endogenous levels of RSK1, RSK2, and RSK3 proteins. In Vero E6 cells, the band of RSK1 was stronger than that of RSK2 as described in the text. The weak bands were enhanced using Adobe Photoshop.

Ltd, Tokyo, Japan). The amount of p90RSK1 in subconfluent cells, p90RSK2 in confluent cells and p90RSK2 in subconfluent cells were 73.05%, 39.94% and 14.70% of RSK1 in confluent cells, respectively. Although affinity of each antibody is different, this result suggested that p90RSK1 was expressed stronger than p90RSK2 in Vero E6 cells. p90RSK1 is expressed mainly in the human kidney, lung, and pancreas, whereas p90RSK2 is expressed in skeletal muscle, heart, and pancreas [33]. p90RSK3 and 4 were not detected in Vero E6 and HeLa cells in the present study. The p90RSK4 was weakly detected in K562 and Jurkat cells.

We examined the phosphorylation status of p90RSK Ser221 in Vero E6 cells. Our previous study indicated that very low levels of Akt in confluent Vero E6 cells are phosphorylated at serine, whereas the level is high in subconfluent cells [28]. However, the phosphorylated threonine of Akt is difficult to detect in subconfluent Vero E6 cells. We only detected it weakly when the cells were treated with epidermal growth factor (EGF) at 1 min [28]. As threonine of Akt was transiently phosphorylated by EGF treatment, it was never detected after 5 min. On the other hand, serine of Akt was easily phosphorylated by treatment with EGF after 3 min. The threonine residue of Akt is phosphorylated by PDK-1, and the serine residue of Akt is thought to be phosphorylated by the putative kinase, PDK-2. To compare the phosphorylation level of PDK-1 at different cell densities, Vero E6 cells were prepared at 10, 5, 2.5, 1.25, 0.6, and 0.3×10^5 cells in 5% FBS containing DMEM per well in 6-well plates. At a density of 10×10^5 cells, Vero E6 cells showed 100% confluence in this experiment. As shown in Fig. 3A, the level of PDK-1 phosphorylation was similar at all cell densities. Ser221 of p90RSK was also phosphorylated at a similar level. The confluency of Vero E6 cells in the present study is shown in Fig. 3B. To confirm that the